UNCLASSIFIED

ISC-729

I

PHYSICS

UNITED STATES ATOMIC ENERGY COMMISSION

FERROMAGNETIC-ANTIFERROMAGNETIC PHASE TRANSITIONS

By
Thomas James Hendrickson
J. M. Keller

March 1956

Ames Laboratory
Iowa State College
Ames, Iowa

Technical Information Service Extension, Oak Ridge, Tenn.

UNCLASSIFIED

DISCLAIMER

II

Work performed under Contract No. W-7405-eng-82.

This report has been reproduced directly from the best available copy.

Printed in USA. Price 60 cents. Available from the Office of Technical Services, Department of Commerce, Washington 25, D. C.

AEC Technical Information Service Extension
Oak Ridge, Tennessee

TABLE OF CONTENTS

FERROMAGNETIC-ANTIFERROMAGNETIC PHASE TRANSITIONS[1]

by

Thomas James Hendrickson and J. M. Keller

ABSTRACT

The problem of ferromagnetic-antiferromagnetic phase transitions for a system in which the angular momentum per atom has the magnitude J is studied in the molecular field approximation. Both ferromagnetic and antiferromagnetic interatomic interactions, which are slightly temperature dependent, are assumed to exist between certain nearby neighbor atoms. An anisotropy energy is introduced of the form which arises from the effect of crystal fields. The structure is subdivided into sublattices, and the partition function **Z** is derived. From **Z** are obtained the free energy F and the equations which determine the average angular momentum per atom of each of the sublattices.

Under the assumption that only first, second, and third nearest neighbor interactions are significant, various ordered arrangements are found for the hexagonal close-packed structure, when it is subdivided into six and into eight hexagonal sublattices and the applied magnetic field is zero.

The molecular field equations are solved for arbitrary magnitudes and directions of the applied magnetic field and for arbitrary temperatures, under the assumption that there are only two inequivalent angular momentum orientations in the crystal, so that the structure may be subdivided into just two sublattices. The relative stability of the various ordered states is investigated.

This report is based on a Ph.D thesis by Thomas James Hendrickson submitted March, 1956 to Iowa State College, Ames, Iowa. This work was performed under contract with the Atomic Energy Commission.

ABSTRACT (Cont.)

Calculations are made for J=15/2, which correspond to the case of dysprosium metal. The parameters giving the magnitude and temperature dependence of the molecular field coefficients are chosen so that the ferromagnetic-antiferromagnetic transition temperature, the Néel temperature, and the paramagnetic Curie temperature coincide with the values for dysprosium. The coefficient giving the magnitude of the anisotropy is selected so that the phenomenon of "spin flop" occurs for magnetic fields of the correct order of magnitude.

The theory predicts the following effects for single crystals. For temperatures in the antiferromagnetic range, a large anisotropy in the single cyrstal susceptibility is expected. The parallel susceptibility, for weak fields parallel to the preferred axis of alignment of the angular momenta, behaves like that of a normal antiferromagnetic, decreasing steadily with decreasing temperature. The perpendicular susceptibility, for weak fields perpendicular to the preferred axis, increases strongly and monotonically as the temperature decreases. For temperatures in the antiferromagnetic range and for magnetic fields making small angles with the preferred axis, the phenomenon of "spin flop" occurs. The angular momenta undergo a sudden change in their directions of alignment as the applied magnetic field increases through a critical value and the corresponding magnetization curves are discontinuous. The temperature of the ferromagnetic-antiferromagnetic transition in magnetic fields parallel to the preferred axis is a strong function of the applied field, increasing with increasing field. For magnetic fields which exceed a certain critical value, the ferromagnetic-antiferromagnetic transtion does not occur at all, and the system remains in the ferromagnetic arrangement for all temperatures.

ABSTRACT (Cont.)

The following results are obtained for polycrystalline dysprosium. The experimentally measured susceptibility, which for a polycrystalline sample is a weighted average of the susceptibilities parallel and perpendicular to the preferred axis in a single crystal, goes through a minimum at a temperature slightly below the Néel temperature, and then increases to very large values as the temperature decreases toward the temperature of the ferromagnetic-antiferromagnetic transition. The theoretical polycrystalline susceptibility shows qualitatively the same behavior. The sharp peak in the heat capacity at the temperature of the ferromagnetic-antiferromagnetic transition should become smeared out in the presence of large external magnetic fields. This should happen because the transition temperature for a single crystal depends strongly upon the orientation of the magnetic field relative to the crystal. A similar effect should appear at the Néel temperature, except that there the effect is less pronounced.

I. INTRODUCTION

Dysprosium metal, which is ferromagnetic below 85°K, has an anomalous peak in magnetic susceptibility near 177°K discovered by Trombe (1), which led him to conclude that the metal is antiferromagnetic between 85 and 177°K. Trombe (2) has summarized in a recent article the magnetic properties of metallic dysprosium. He reports that between 730 and 177°K the element is paramagnetic with a paramagnetic Curie temperature of 157°K and a magnetic moment per atom of approximately 10.64 Bohr magnetons. A very sharp peak in the curve of the susceptibility vs. temperature is observed near 177°K. The susceptibility decreases as the temperature decreases from 177 to about 160°K, where it passes through a minimum. Below 160°K, the susceptibility increases rapidly with decreasing temperature, suggesting the approach to a ferromagnetic Curie point. The temperature of the ferromagnetic-antiferromagnetic transition depends strongly on the magnitude of the applied magnetic field.

Trombe's work was confirmed by Elliott, Legvold, and Spedding (3), who extended the measurements to lower temperatures and higher magnetic fields. Their high field measurements show saturation effects for temperatures between 85 and 176°K and suggest that for strong fields dysprosium may never become antiferromagnetic. The heat capacity of dysprosium, which was measured by Griffel, Skochdopole, and Spedding

(4), has sharp peaks at 174 and 83.5°K. It is apparent that a magnetic ordering transition occurs at 174°K, since the heat capacity peak at this temperature is very high, much higher than the peak at 83.5°K, the temperature where the system becomes ferromagnetic. For the complete temperature interval between 40 and 300°K, dysprosium has the hexagonal close-packed structure (5), so that the specific heat peaks and magnetic anomalies are not associated with changes in crystal structure. The magnetic behavior and heat capacity of dysprosium indicate that the metal is successively ferromagnetic, antiferromagnetic, and paramagnetic as the temperature increases from below 85°K to above 176°K.

In our work, which is motivated by the above results for the properties of dysprosium, we study in the molecular field approximation the theory of ferromagnetic-antiferromagnetic transitions for the hexagonal close-packed structure. We assume that there are both ferromagnetic and antiferromagnetic interatomic interactions in the system, as well as an anisotropy energy which determines the axis of alignment of the system in zero applied magnetic field. We find, in this approximation, that the system can order in ferromagnetic and in several kinds of antiferromagnetic arrangements. We also find that, with certain restrictions, ferromagnetic-antiferromagnetic transitions can occur only if the molecular field coefficients for the interactions between atoms vary with temperature. This result agrees with that of Smart (6),

which was derived for the special case where the spin per atom is $\frac{1}{2}$.

We assume that the molecular field coefficients vary slightly with temperature and solve the molecular field equations for large applied magnetic fields making an arbitrary angle with the preferred axis of alignment of the system. We compare the results of the calculations with experiment and predict some effects which can be looked for experimentally in the magnetic behavior of single crystals and in the heat capacity of both single crystals and polycrystalline samples in the presence of a magnetic field.

II. REVIEW OF THEORY AND LITERATURE SURVEY

We describe briefly the present situation in the theories of ferromagnetism and antiferromagnetism, before going on to develop from the standpoint of the molecular field theory the basic equations which we use in the discussion of ferromagnetic-antiferromagnetic transitions.

In order to account for the appearance of spontaneous magnetization in ferromagnetics, P. Weiss (7) assumed that the magnetic effects of the interactions between atoms could be represented by an effective molecular field proportional to the magnetization, of the form

$$H_e = N_W m \ , \qquad (2.1)$$

where H_e is the effective field, N_W is the Weiss molecular field coefficient, and m is the average magnetization per atom. According to the Weiss theory, the total field H_t experienced by a given atom can be written

$$H_t = H + N_W m \ , \qquad (2.2)$$

where H is the external field. If the necessary modifications are made to the Weiss molecular field treatment to include quantum mechanical effects, the magnetization m is given by

$$m = \mu \, B_J(\mu H_t / kT) \ , \qquad (2.3)$$

where $\mu = g_J \mu_B J$, g_J is the Landé g-factor for angular momentum

J, μ_B is the Bohr magneton, and B_J is the Brillouin function for angular momentum J, defined by

$$B_J(y) = \frac{2J+1}{2J} \coth \frac{(2J+1)y}{2J} - \frac{1}{2J} \coth \frac{y}{2J} . \qquad (2.4)$$

A fundamental explanation of the origin of the Weiss molecular field was first given by Heisenberg (8) in 1928 in terms of exchange interactions, which are equivalent to an interatomic potential of the form

$$V_{ij} = - J_{ij}(1+4\vec{S}_i.\vec{S}_j)/2 , \qquad (2.5)$$

where $\vec{S}_i$ and $\vec{S}_j$ are the spin angular momentum vectors of atoms i and j measured in units of $h/2\pi$, h is Planck's constant, and J_{ij} is the exchange integral for the interaction between atoms i and j. If the sign of J_{ij} is positive, the interaction between atoms i and j is ferromagnetic in nature, since the energy of interaction is lowest when the spins are parallel. Conversely, if J_{ij} is negative, the interaction is antiferromagnetic in character.

The theory of cooperative phenomena, of which ferromagnetism and antiferromagnetism are typical examples, is one of the most difficult fields of statistical mechanics. The study of magnetic ordering is greatly complicated because the spin vectors appearing in Eq. (2.5) are quantum mechanical operators. Many approximations have been employed for the study of ferromagnetism and antiferromagnetism, some being valid for high temperatures, others for temperatures near the

absolute zero. One of the principal high temperature approximations is the Bethe-Peierls approximation, which has been applied to the study of ferromagnetism by P. R. Weiss (9) and to antiferromagnetism by Li (10). These approximations are successful in predicting that one- and two-dimensional lattices will not be ordered, and in obtaining reasonable values for the critical temperatures for the simple cubic and body-centered cubic structures. They also take into account successfully short range order effects. However, Anderson (11) has shown that, in the ferromagnetic case, the Bethe-Peierls-Weiss method breaks down for temperatures of the order of half the critical temperature. Since there is doubt concerning the validity of the method for temperatures much below the critical temperature, and since it becomes exceedingly complicated to apply in the case of interactions between more than one kind of neighbor, we think it unwise to employ the Bethe-Peierls-Weiss approximation for our investigation of the theory of ferromagnetic-antiferromagnetic transitions.

The theory of ferromagnetism at low temperatures has been treated successfully by the spin wave theory originated by Bloch (12), in which the deviations of the spins from what would be expected in a state of perfect order are studied. The spin wave theory predicts the correct $T^{3/2}$ behavior of the approach of the magnetization to saturation for low temperatures. The most recent discussion of the spin wave

theory of ferromagnetism is by Marshall (13), who points out that it is a rigorous theory for ferromagnetism because the exact ground state for the system is known and because it can be proved that the approximations employed have no important effects in the limit of very low temperatures.

Marshall (13), also discusses the spin wave theory of antiferromagnetism and emphasizes that it is much less well founded. He points out that it has been impossible to demonstrate conclusively that the approximations used in the spin wave method do not affect the validity of the results. In an earlier paper, Marshall (14) showed that, in contrast to the situation for ferromagnetics, the ground states for antiferromagnetics have never been derived rigorously. The review article of Nagamiya, Yosida, and Kubo (15), provides an extensive discussion of the spin wave theory of antiferromagnetism as it has been developed by many workers. The spin wave theory, since it is appropriate only for very low temperatures, cannot be used in our discussion of the theory of ferromagnetic-antiferromagnetic transitions, which occur at rather high temperatures.

The molecular field approximation, which we use to study ferromagnetic-antiferromagnetic (F-A) transitions, has been applied widely to antiferromagnetism and provides a good semi-quantitative description of many phenomena. Néel (16), in 1932, first adapted the concept of the Weiss molecular field to antiferromagnetism, and since then his original

ideas have been extended and refined by many workers, including Van Vleck (17), Anderson (18), Smart (19), and Nagamiya (20). Excellent reviews of the whole field of antiferromagnetism have been published by Van Vleck (21), Lidiard (22), and Nagamiya, Yosida, and Kubo (15).

The molecular field theory corresponds to the Bragg-Williams approximation in the theory of order-disorder in alloys (23, p. 791), and to the first Heisenberg approximation in the theory of ferromagnetism (24, p. 329). Although it represents the crudest approximation in the theory of cooperative phenomena, it has had remarkable success in describing the properties of antiferromagnetics, and furthermore, it has the useful property of being applicable for all temperatures. A detailed discussion of the molecular field approximation is given in Chapter III, along with derivations of the molecular field equations and the free energy of the system.

The problem of F-A transitions has been studied in the molecular field approximation by Smart (6) and by Elcock (25) for the special case of spin $\frac{1}{2}$. They both arrived at the conclusion that F-A transitions can occur only if the molecular coefficients for the interatomic interactions are slightly temperature dependent. Smart (6) derived the free energy of the system by writing down for the entropy S,

$$S = k \ln W(M_1,\ldots,M_n) , \qquad (2.6)$$

where $W(M_1,\ldots,M_n)$ is the total number of ways of orienting the atomic spins on the lattice sites of the n sublattices into which the structure is subdivided consistent with the equilibrium values of the magnetizations M_i of the sublattices. The M_i are found from the standard equations of the molecular field approximation. For spin $\frac{1}{2}$, $W(M_1,\ldots,M_n)$ is known in closed form and $\ln W(M_1,\ldots,M_n)$ can be approximated by using the Stirling formula for the factorials involved. Smart determined the Gibbs free energy G for zero applied magnetic field by integrating the thermodynamic relation

$$dG = - S\, dT \quad , \qquad (2.7)$$

where T is the temperature and the molecular field coefficients vary with T. Elcock (25) has criticized Smart's derivation and given one of his own which starts from the partition function Z. Our derivation of the molecular field equations starts from the partition function Z in the same manner as Elcock, and differs only in detail because we are dealing with ions of arbitrary angular momentum J, rather than the case $J = \frac{1}{2}$ studied by Elcock. We believe that our method, which is based in part on the derivation for arbitrary J of the partition function for a ferromagnetic system described by Van Vleck (24, p. 329), has the advantage of bringing out clearly the origin and significance of the effective field felt by the atoms of each sublattice.

Yaffet and Kittel (26), also using the molecular field

approximation, have studied the theory of magnetic structure transitions in ferrites, where transitions can occur even when the molecular field coefficients are independent of temperature. The ferrites have the spinel structure, in which the magnetic ions are distributed among two inequivalent sites A and B. The magnetic ions can be of different kinds on the two sites. Yaffet and Kittel examined the free energy at absolute zero and obtained the condition which determines the stable configuration for different concentrations of magnetic ions and different magnitudes of the field coefficients. They also derived the condition which determines the state which has the highest critical temperature and is therefore stable at high temperatures. They showed there was no necessary relation between the two conditions and that therefore the possibility existed that transitions between various ordered states could occur, even if the molecular field coefficients were independent of the temperature.

Molecular field equations similar to ours have been studied, again for $J = \frac{1}{2}$, using further approximations which are not appropriate for the range of temperatures and magnetic fields needed to describe the properties of dysprosium. Gorter and Haantjes (27) have studied the molecular field equations for a system rather similar to ours, but they have introduced anisotropy effects by assuming an anisotropic g-factor and anisotropic exchange interactions, instead of assuming as we have that the anisotropy arises through crystal fields.

Furthermore, their methods, although they are valid for all magnitudes of the applied magnetic field, work only for the absolute zero of temperature. Yosida (28) and Poulis and Hardemann (29) have studied systems having the same form of anisotropy as we have assumed, but their approximations, while good for a wide range of temperatures, appear to be valid only for small magnetic fields. Their model differs from ours in that they have considered only antiferromagnetic interatomic interactions, while we have assumed that ferromagnetic interactions are also present. The phenomenon of "spin flop" which appears in our model has been described in the review articles of Nagamiya, Yosida, and Kubo (15) and of Poulis and Gorter (30).

III. THE MOLECULAR FIELD APPROXIMATION

We use the following model to investigate the magnetic properties of the rare earth metals. Each atom is considered to exist in the metal as a tripositive ion in the same spectroscopic level as the free ion given by Hund's rule. We assume that the ith and jth atoms interact with an isotropic interaction, which can be written

$$V_{ij} = - g_j \mu_B H_{ij} \vec{J_i} \cdot \vec{J_j} , \qquad (3.1)$$

where g_J is the Lande g-factor for angular momentum J, μ_B is the Bohr magneton, H_{ij} is the coefficient for the interaction between the ith and jth atoms, and vector $\vec{J_i}$ represents the angular momentum of the ith atom in units of $h/2\pi$. The magnitude of $\vec{J_i}$ is given by the quantum number J, so that $\vec{J_i}^2 = J(J+1)$.

We assume that the anisotropy energy of the ith atom due to crystal fields can be written in terms of J_{iz}, the z component of the angular momentum J_i, as

$$- g_J \mu_B (K/2) J_{iz}^2 , \qquad (3.2)$$

where K is a constant which has the dimensions of a magnetic field and gives the magnitude of the anisotropy. A discussion of the anisotropy energy is given in Appendix A. The energy of the ith atom due to an applied magnetic field H is written in the customary form

$$- g_J \mu_B \vec{J}_i \cdot \vec{H} , \qquad (3.3)$$

where $\vec{H}$ is the external field.

We write for the total energy E of the system, therefore,

$$E = - g_J \mu_B \left[\sum_{i>j} H_{ij} \vec{J}_i \cdot \vec{J}_j + \vec{H} \cdot \sum_i \vec{J}_i + \sum_i (K/2) J_{iz}^2 \right] . \qquad (3.4)$$

In the molecular field method, the energy E of Eq. (3.4) is approximated in a manner which we now describe. Assume that the coefficients H_{ij} are zero for all pairs of atoms which are more distant from each other than rth nearest neighbors. Then subdivide the structure into sublattices in such a manner that no sublattice contains atoms which are nearer to each other than (r+1)th nearest neighbors, and no sublattice contains more than one kind of neighbor of the atoms of any other sublattice. In general there are many different ways of subdividing a structure, depending on its symmetry and the relative importance of the interactions between different kinds of neighbors. Let us assume that there are 2N atoms per sublattice and that there are n sublattices.

Now consider the energy of interaction of an atom on the ith sublattice with its neighbors on the jth sublattice. This energy is

$$g_J \mu_B \vec{J}_i \cdot \sum_{(k)} H_{ik} \vec{J}_k , \qquad (3.5)$$

where the summation is over all the interacting neighbors of the atom on the ith sublattice which reside on the jth sub-

lattice. The coefficients H_{ik} are the same for all interacting pairs. In the molecular field approximation this energy is written in the form

$$g_J\mu_B z_{ij} H_{ij} \vec{J_i}\cdot\vec{S_j} = g_J\mu_B \gamma_{ij} \vec{J_i}\cdot\vec{S_j} , \qquad (3.6)$$

where $\vec{S_j}$ denotes the average angular momentum per atom of the jth sublattice, given by

$$2N \vec{S_j} = \sum_{(k)} \vec{J_k} . \qquad (3.7)$$

The symbol z_{ij} gives the number of atoms on the jth sublattice which interact with a given atom on the ith sublattice, and we have taken $\gamma_{ij}=z_{ij}H_{ij}$. We now approximate Eq. (3.4) by

$$E = - 2Ng_J\mu_B\left[\sum_{i>j}\gamma_{ij}\vec{S_i}\cdot\vec{S_j} + \vec{H}\cdot\sum_i\vec{S_i} + \sum_i (K/2)S_{iz}^2\right]. \qquad (3.8)$$

Here, in contrast to Eq. (3.4), the summations are over the several different sublattices, so that i and j range from 1 to n. The vectors $\vec{S_i}$ and $\vec{S_j}$ represent the average angular momenta of the ith and jth sublattices, respectively.

In the molecular field approximation, the long range order of the system is taken into account by subdividing the structure into sublattices. It is assumed in writing down Eq. (3.8) that the total energy E is a function only of the average angular momenta of the sublattices, and therefore of the long range order of the system. This is a serious assumption and much more drastic than our earlier assumption that we need consider only interatomic interactions between

certain nearby neighbors. Specifically, it neglects short range order. It is apparent that with short range interactions there exists for a given set of values for the average angular momenta of the sublattices a wide range of energies for the system. This failure to take account properly of short range effects is most serious for temperatures very near and slightly above a critical temperature. For temperatures well below a critical temperature, the system is strongly ordered, so that the assumption that it is the long range order which is important in determining the orientation of a given spin seems to be reasonable. At any rate, the already considerable success of the molecular field approximation in interpreting the experimental results for antiferromagnetism recommends its continued use, especially when the rather severe mathematical difficulties of the more exact theories are recalled.

The partition function Z for the system is

$$Z = \sum_{\vec{S}_1,\ldots,\vec{S}_n} \exp(-E/kT) , \qquad (3.9)$$

where the summations are over all the magnitudes and directions of the sublattice vectors $\vec{S}_i$. The summations in Eq. (3.9) can be performed approximately if we assume that the principal contributions come from values of the $\vec{S}_i$ near certain mean values $\vec{S}_i^*$. The method for finding the $\vec{S}_i^*$ is described later. If the energy E of Eq. (3.8) is expanded in a Taylor's series about the mean values $\vec{S}_i^*$ and only terms linear in $(\vec{S}_i - \vec{S}_i^*)$

are retained, E takes the form

$$E = - E^* - 2Ng_J\mu_B\sum_i \vec{S}_i.\vec{H}_i \quad , \tag{3.10}$$

where

$$E^* = - 2Ng_J\mu_B \sum_i (K/2)S_{iz}^{*2} + \sum_{i>j}\gamma_{ij}\vec{S}_i^*.\vec{S}_j^* \quad , \tag{3.11}$$

and

$$\vec{H}_i = \vec{H} + \sum_j{}'\gamma_{ij}\vec{S}_j^* + KS_{iz}^*\hat{z} \quad . \tag{3.12}$$

The symbol $\sum_j{}'$ means to sum over j leaving out the term i=j, and $\hat{z}$ is the unit vector parallel to the positive z axis. The field $\vec{H}_i$ is the effective field felt by the atoms of the ith sublattice.

The partition function Z of Eq. (3.9) can be written

$$Z = \exp(E^*/kT)\pi_i Z_i \quad , \tag{3.13}$$

where

$$Z_i = \sum_{\vec{S}_i} \exp\left[(2Ng_J\mu_B/kT)\vec{S}_i.\vec{H}_i\right] \quad . \tag{3.14}$$

The summation in Eq. (3.14) is over all magnitudes and directions of the $\vec{S}_i$, corresponding to all possible orientations of the 2N ions that make up the ith sublattice. A convenient way to perform the sum for the ith sublattice is to choose the direction of the effective field $\vec{H}_i$ as the direction of quantization of the angular momenta for the ith sublattice and to classify the states of the sublattice by

the projections of their total angular momenta in the direction of H_i. To use this technique we transform Eq. (3.14) into

$$Z_i = \sum_i w(M_i) \exp \left[(\mu M_i H_i)/(JkT) \right] , \qquad (3.15)$$

where $\mu = g_J \mu_B J$, M_i is the projection of the total angular momentum of sublattice i along the field $\vec{H_i}$, and H_i is the magnitude of $\vec{H_i}$. The factor $w(M_i)$ is the number of ways that 2N ions each of angular momentum J can be arranged so that the total component of the angular momentum along the direction of quantization is M_i. It can be shown (24, p. 324) that $w(M_i)$ is the coefficient of X^{M_i} in the expansion of $(X^J+X^{J-1}+.....+X^{-J})^{2N}$. The result of the summation is that

$$Z_i = Z_i(y_i) = \left[\sinh \frac{(2J+1)y_i}{2J} \Big/ \sinh \frac{y_i}{2J} \right] 2N , \qquad (3.16)$$

where $y_i = \mu H_i/kT$. The free energy F is given by the usual relation

$$F = - kT \ln Z, \qquad (3.17)$$

which from Eq. (3.13) is

$$F = - E^* - kT \sum_i \ln Z_i . \qquad (3.18)$$

We find $\vec{S_i}^*$, the mean value of $\vec{S_i}$, from the relation

$$\vec{S_i}^* = Z^{-1} \sum_{\vec{S_1},\ldots,\vec{S_n}} \vec{S_i} \exp(-E/kT), \qquad (3.19)$$

in which the summations may be carried out with the same approximations used in calculating Z.

Observe that the summation to be carried out in Eq. (3.15) is identical with the summation which must be carried out in the derivation of the partition function for a dilute paramagnetic system of ions with permanent magnetic moments μ in the presence of an external magnetic field, where now the effective field H_i plays the role of the external magnetic field. Therefore, the partition function Z_i is identical with the partition function for a dilute paramagnetic system in an external field H_i (23, p. 468). This identity comes about because of the linearization approximation used in obtaining the form (3.13) for the partition function Z, since this approximation replaces the interaction between sublattices by an effective field. This type of approximation - in one form or another - is at the heart of all molecular field treatments. By comparing Eqs. (3.14) and (3.19), we see that S_i^*, the magnitude of $\vec{S_i}^*$, can be obtained formally from the relation

$$S_i^* = (kT/2Ng_J\mu_B)\,\partial \ln Z/\partial H_i = J\,B_J(\mu H_i/kT) \quad , \qquad (3.20)$$

where the Brillouin function B_J is given in Eq. (2.4). Keeping in mind our above remarks, we see the physical significance of $\vec{S_i}^*$. It is a vector parallel to $\vec{H_i}$, whose magnitude represents the average projection per atom of the angular momentum of the ith sublattice in the direction of $\vec{H_i}$. This result follows from Eq. (3.19), because all vectors having the same magnitude and making equal angles

with $\vec{H}_i$ have equal weights in the sum, so that the sum of their components perpendicular to $\vec{H}_i$ is zero.

The ordered states of the system are found by solving Eqs. (3.20), which are a set of transcendental equations; the effective field $\vec{H}_i$ is given by Eq. (3.12). The free energy F of Eq. (3.18) reduces to the free energy derived by Smart (6) and Elcock (25) for the special case of $J=\frac{1}{2}$ and zero external magnetic field, if the molecular field coefficients γ_{ij} are independent of temperature. With the help of Eqs. (3.11) and (3.12), we write Eq. (3.18) in the useful form

$$F = \sum_i F_i - Ng_J\mu_B \vec{H} \cdot \sum_i \vec{S}_i^* \quad , \tag{3.21}$$

where

$$F_i = Ng_J\mu_B \vec{S}_i^* \cdot \vec{H}_i - kT \ln Z_i \quad . \tag{3.22}$$

Since all our equations involve the mean values $\vec{S}_i^*$, it is convenient to discard the asterisk in all subsequent work, with the understanding that the symbol $\vec{S}_i$ means the statistical mechanical average angular momentum per atom of the ith sublattice.

IV. SOLUTIONS FOR ZERO EXTERNAL MAGNETIC FIELD

We have derived in Chapter III the basic equations of the molecular field approximation. The magnitude of the angular momentum S_i of atoms on sublattice i is obtained from the equation

$$S_i = J\, B_J(\mu H_i/kT) \,, \tag{3.20}$$

while the effective field $\vec{H_i}$ is given by

$$\vec{H_i} = \vec{H} + \sum_j{}' \gamma_{ij} \vec{S_j} + K\, S_{iz}\, \hat{z} \,. \tag{3.12}$$

Equations (3.20) and (3.12) comprise a set of simultaneous, transcendental equations which are subject to the condition that the $\vec{S_i}$ be parallel to the effective field $\vec{H_i}$. This condition, expressed by the equation

$$\vec{H_i} = \lambda_i \vec{S_i} \,, \tag{4.1}$$

arises in the molecular field approximation because the sublattice angular momentum $\vec{S_i}$ is the statistical average of the projections of the angular momenta of the individual atoms of the ith sublattice in the direction of the effective field $\vec{H_i}$.

Substitute Eqs. (4.1) in Eqs. (3.12) to obtain the set of equations

$$\lambda_i \vec{S_i} - \sum_j{}' \gamma_{ij} \vec{S_j} - K\, S_{iz}\, \hat{z} = \vec{H} \,, \tag{4.2}$$

where the magnitude S_i is now given by

$$S_i = J\, B_J(\mu\lambda_i S_i/kT) \quad . \tag{4.3}$$

We seek solutions of Eqs. (4.2) and (4.3) with the lowest free energy F of Eq. (3.21) for a given H and T. In Appendix D are given graphs of $B_J(x)$ plotted against x and of (S_i/J) plotted against $(C'\lambda_i/T)$, where $C'=g_J\mu_B J(J+1)/3k$.

We now investigate the nature of the ordered states of the system in zero external magnetic field. A class of solutions of Eqs. (4.2) with H=0 can be found for which all the λ_i have the same value λ. It is believed that this class of solutions contains in every case the solution of lowest free energy. But it is not evident how to prove this contention without examining each possibility in turn. Appendix B contains a discussion of this question, in which it is shown that under certain conditions the state with the lowest free energy is one for which all the λ_i have the same value. But we have not exhausted all possibilities.

If we set H=0 in Eq. (4.2) and assume that $\lambda_i=\lambda$, for all i, Eqs. (4.2) become a set of homogeneous equations which have non-trivial solutions if either

$$\left|\lambda\delta_{ij} - \gamma_{ij}\right| = 0 \quad , \tag{4.4}$$

or

$$\left|(\lambda - K)\,\delta_{ij} - \gamma_{ij}\right| = 0 \quad , \tag{4.5}$$

where δ_{ij} is the Kronecker delta. Corresponding to each λ,

which is a solution of Eq. (4.4), there exists one or more ordered states for which the $\vec{S}_i$ are aligned perpendicular to the z axis, while for each λ satisfying Eq. (4.5) there exists one or more ordered states for which the $\vec{S}_i$ are aligned along the z axis.

From the λ's which solve Eqs. (4.4) and (4.5), we can find the critical temperatures for the various ordered states, where we define the critical temperature for an ordered state as the temperature below which the state becomes stable relative to a random arrangement. The critical temperature T_c, the temperature below which transcendental equation (4.3) has a solution other than the trivial solution $S_i=0$, can be found by differentiating both sides of Eq. (4.3) with respect to S_i and setting $S_i=0$. By this procedure, which is described further in Appendix D, we find

$$T_o = \lambda C' \quad , \tag{4.6}$$

where $C' = g_J \mu_B J(J+1)/3k$.

We now specialize the discussion to the hexagonal close-packed structure of dysprosium. We divide the structure into at least eight sublattices, in order to take into account interactions between first, second, and third nearest neighbors. We assume that more distant neighbor interactions can be neglected. The (c/a) ratio for dysprosium, which has been measured by Banister, Legvold, and Spedding (5), ranges between 1.581 for 48°K and 1.571 for 302°K. The (c/a) ratio

is 1.63 for the case of ideal close packing, where the twelve nearest neighbors of a given atom are all at the same distance away. Therefore, the six nearest neighbors of an atom in a certain (001) plane lie in adjacent (001) planes, which also contain the six third nearest neighbors. The six second nearest neighbors lie in the same (001) plane as the atom in question. For this present work, we subdivide the structure into eight hexagonal sublattices. A convenient method for enumerating the sublattices is described below. Sublattices 1, 3, 5, and 7 are taken so that they have atoms in the same (001) planes. Now sublattice 2 is chosen to contain the third nearest neighbor atoms for sublattice 1; 4 those for 3; and so on. This enumeration is illustrated in Fig. 1.

Let $p/2$ be the Weiss molecular field coefficient (the H_{ij}) for the interaction between atoms which are second nearest neighbors, and $q/2$ that for nearest neighbors. Let $r/6$ be the coefficient for third nearest neighbors. Thus if we consider an atom on a certain sublattice, its six nearest neighbors are arranged on three sublattices, each containing two nearest neighbors. For example, sublattice 4 contains two nearest neighbors of an atom on sublattice 1, so that the coefficient γ_{14} is $2(q/2)=q$, where γ_{14} is defined in Eq. (3.6). Similarly, the coefficient γ_{ij} has the value p for the interaction between sublattices which contain second nearest neighbors of each other. Since the six third nearest neighbors of a given atom all lie on a single sublattice, γ_{ij} has

Fig. 1. Sublattice arrangement for the hexagonal close-packed structure when subdivided into eight hexagonal sublattices. The atoms designated by ○ lie in the same (001) plane, while the atoms designated by □ lie in adjacent (001) planes which do not contain the ○ atoms.

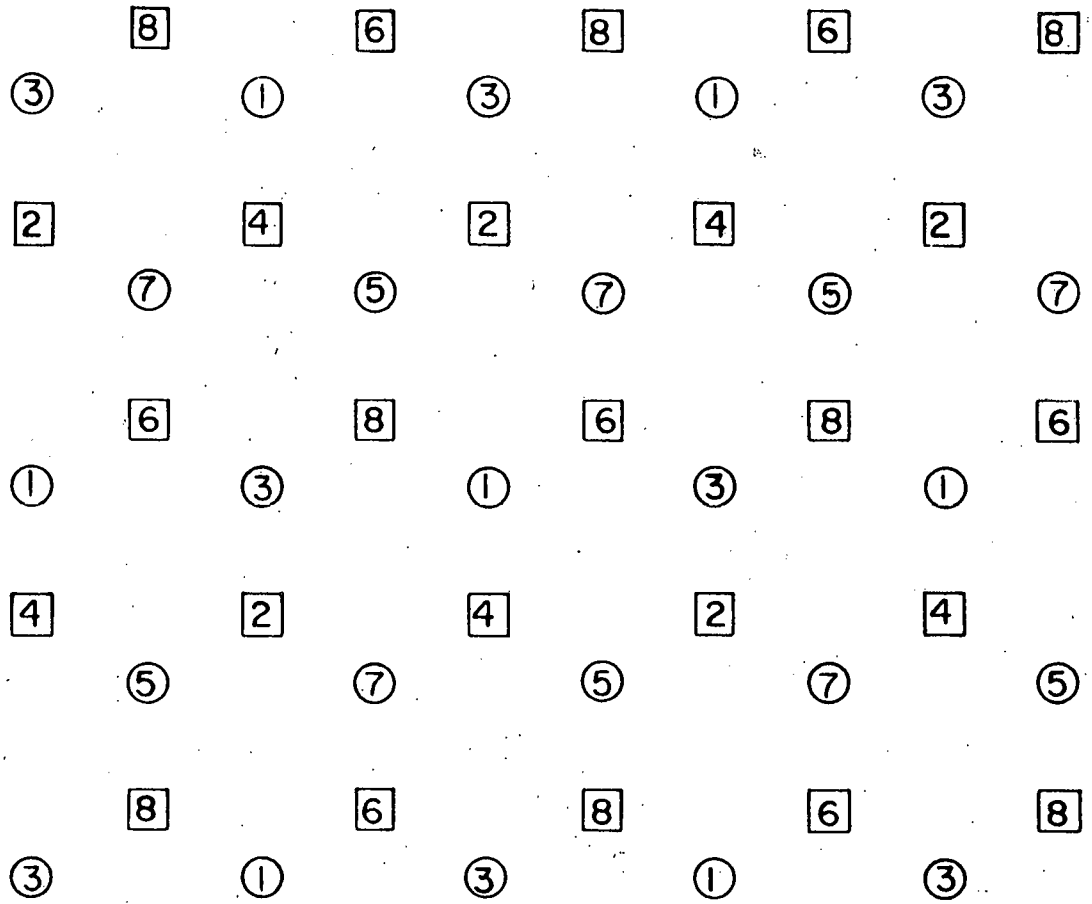
8 6 8 6 8
3 1 3 1 3
2 4 2 4 2
7 5 7 5 7
6 8 6 8 6
1 3 1 3 1
4 2 4 2 4
5 7 5 7 5
8 6 8 6 8
3 1 3 1 3

the value r for the interaction between sublattices which contain atoms which are third nearest neighbors.

The secular equation for the above arrangement of sublattices, as obtained from Eq. (4.4), is

$$\begin{vmatrix} -\lambda & r & p & q & p & q & p & q \\ r & -\lambda & q & p & q & p & q & p \\ p & q & -\lambda & r & p & q & p & q \\ q & p & r & -\lambda & q & p & q & p \\ p & q & p & q & -\lambda & r & p & q \\ q & p & q & p & r & -\lambda & q & p \\ p & q & p & q & p & q & -\lambda & r \\ q & p & q & p & q & p & r & -\lambda \end{vmatrix} = 0, \qquad (4.7)$$

where p, q, and r are described above. Equation (4.7) can be factored into

$$\left[\lambda-3(p+q)-r\right]\left[\lambda-3(p-q)+r\right] \times \left[\lambda+p+q-r\right]^3\left[\lambda+p-q+r\right]^3 = 0 . \qquad (4.8)$$

The factors for Eq. (4.5) can be obtained from Eq. (4.8) by replacing λ by $(\lambda-K)$. The various critical temperatures defined by Eq. (4.6) are given, in units of $C'=g_J\mu_B J(J+1)$, in Table I, along with the types of order with which they are associated. The symbols for the types of order have the following significance. The capital letter gives the type of order, while the subscript x means that the angular momenta are aligned perpendicular to the z axis, and the

subscript z means the angular momenta are aligned along the z axis. The types of order are determined by substituting the appropriate values for λ into Eqs. (4.2) and then solving these equations for the relative values of the angular momentum components.

Table I. Critical temperatures in units of C' for various kinds of order in the hcp structure, when it is subdivided into eight hexagonal sublattices.

Type of Order	T_C/C'
F_x	$3(p+q)+r$
F_z	$3(p+q)+r+K$
A_x	$3(p-q)-r$
A_z	$3(p-q)-r+K$
B_x	$-p-q+r$
B_z	$-p-q+r+K$
C_x	$-p+q-r$
C_z	$-p+q-r+K$

The ordered states listed above are shown in Fig. 2. They can be described as follows. The ferromagnetic state F has the angular momenta of all sublattices aligned parallel to each other. Antiferromagnetic state A has the angular momenta on alternate (001) planes aligned antiparallel to each other. Antiferromagnetic state B is an ordering in which each (001) plane contains equal numbers of angular

Fig. 2. Ordered states for the hcp structure subdivided into the eight sublattices shown in Fig. 1. The symbols ○ and □ denote angular momenta pointing parallel to a given direction, ● and ■ denote angular momenta pointing antiparallel to that direction.

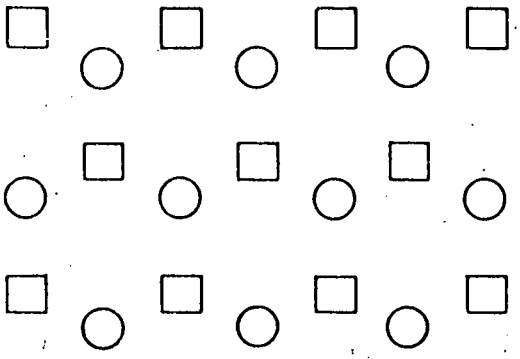

STATE F

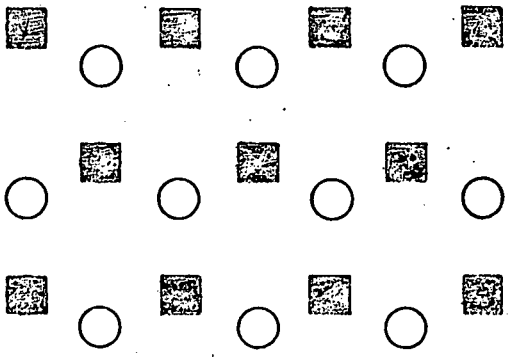

STATE A

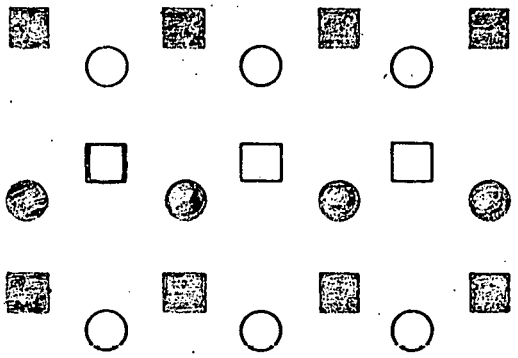

STATE B

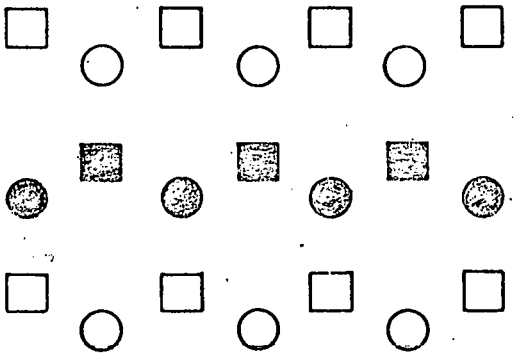

STATE C

momenta aligned parallel and anti-parallel to a given direction, arranged on a set of parallel lines occupied by angular momenta all of one orientation. Neighboring planes are oriented so that third nearest neighbors have parallel angular momenta. Antiferromagnetic state C has the same arrangement as B within any (001) plane, but adjacent planes are oriented so that third nearest neighbors have antiparallel angular momentum orientations.

In the work above, we have decomposed the hcp structure into eight hexagonal sublattices. This subdivision is appropriate when first, second, and third nearest neighbor interactions are taken into account. If third nearest neighbor interactions can be neglected, another possible subdivision is into six hexagonal sublattices. The atoms in each (001) plane are arranged on three interlocking hexagonal lattices, and since atoms on adjacent planes cannot be on the same sublattice, six sublattices are required.

The formal details of the solution are identical with those for the case of eight sublattices. The secular determinant is

$$\begin{vmatrix} -\lambda & d & d & q & q & q \\ d & -\lambda & d & q & q & q \\ d & d & -\lambda & q & q & q \\ q & q & q & -\lambda & d & d \\ q & q & q & d & -\lambda & d \\ q & q & q & d & d & -\lambda \end{vmatrix} = 0 , \qquad (4.9)$$

where d=3p/2, and p and q have the same significance as in Eq. (4.7). Equation (4.9) can be factored into

$$(\lambda+d)^4(\lambda-2d-3q)\ (\lambda-2d+3q) = 0 \quad . \tag{4.10}$$

The various critical temperatures are given in Table II.

Table II. Critical temperatures in units of C' for the hcp structure subdivided into six hexagonal sublattices.

Type of Order	T_C/C'
F_x	3(p+q)
F_z	3(p+q)+K
A_x	3(p-q)
A_z	3(p-q)+K
D_x	-3p/2

States F_x, F_z, A_x, and A_z are the same states described before and illustrated in Fig. 2. State D_x, however, is a new state of some interest, which is obtained by substituting $\lambda=-d$ into Eqs. (4.2) and solving for the components of the sublattice vectors $\vec{S_i}$. The arrangement of vectors for this case can be found as follows. Equations (4.2) can be written

$$d(S_{1x}+ S_{2x}+ S_{3x}) + q(S_{4x}+ S_{5x}+ S_{6x}) = 0 \ ,$$

$$q(S_{1x}+ S_{2x}+ S_{3x}) + d(S_{4x}+ S_{5x}+ S_{6x}) = 0 \ , \tag{4.11}$$

with similar equations for the y components. Since in general

Fig. 3. Angular momentum arrangement for state D_x in a (001) plane of the hcp structure, when it is subdivided into six hexagonal sublattices.

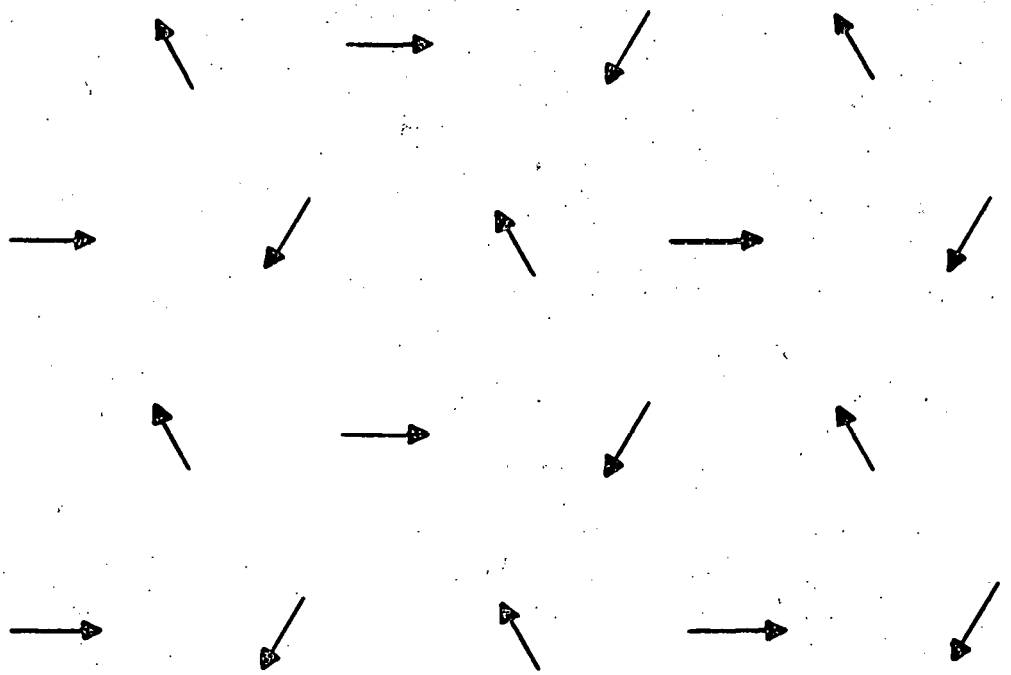

$(d^2 - q^2 \neq 0)$, we see that

$$(S_{1x} + S_{2x} + S_{3x}) = (S_{4x} + S_{5x} + S_{6x}) = 0 ,$$

$$(S_{1y} + S_{2y} + S_{3y}) = (S_{4y} + S_{5y} + S_{6y}) = 0 . \qquad (4.12)$$

For state D_x, the z components of the angular momenta are all zero. The vectors $\vec{S}_i$ all have the same magnitude given by Eq. (4.3). Therefore, it is clear that Eqs. (4.12) are satisfied if we place the vectors in each (001) plane so that they have directions 120° apart. This arrangement of angular momenta is shown in Fig. 3. The total angular momentum of each (001) plane is zero, so that there is no interaction between adjacent (001) planes and therefore no necessary correlation of the angular momentum arrangement between planes. Since for state D_x the third nearest neighbor interactions cancel out, D_x is a possible arrangement even in the presence of strong third nearest neighbor interactions, although it probably would not be the arrangement of lowest free energy.

We have examined above the possible ordered states for the hcp structure, when it is subdivided into six and into eight hexagonal sublattices. These subdivisions are appropriate when interactions between atoms more distant than third nearest neighbors can be neglected. If longer-ranged interactions have to be considered, the structure must be subdivided still further. It does not seem worthwhile to examine more complex structures, unless neutron

diffraction data show they are needed.

We now investigate the relative stabilities of the magnetic states listed in Tables I and II. For H=0, and all λ's equal, the free energy of Eq. (3.21) can be written in the form

$$F = nNg_J\mu_B\lambda S^2 - nkT \ln Z_1(\mu\lambda S/kT) , \qquad (4.13)$$

where n is the number of sublattices and Z_1 is the function $Z_1(y_1)$ defined by Eq. (3.16). Observe that F decreases monotonically as λ increases, so that the state with the largest λ is stable at temperature T. Furthermore, if the λ's are independent of temperature, the state with the largest λ, and consequently the largest critical temperature, remains stable for all temperatures below its critical temperature. Therefore, we conclude that a transition from one ordered state to another listed in Tables I and II can only occur, for the hcp structure in this approximation, when the λ's vary with temperature. This conclusion had been reached earlier by Smart (31) for cubic lattices with $J=\frac{1}{2}$.

The solutions above have been obtained under the assumption that all the λ_i of Eqs. (4.1) and (4.2) are equal when H=0. The problem of whether there are other consistent solutions for H=0 when this assumption is abandoned is examined in Appendix B. It is shown there that if states A and F have positive critical temperatures, while the

critical temperatures for states B and C are negative, both states A and F are more stable at all temperatures than any other solutions of the equations. Therefore, in this special case at least, a ferromagnetic-antiferromagnetic transition can only occur when the molecular field coefficients change with temperature.

Without neutron diffraction data or data from magnetic measurements on single crystals, it is virtually impossible to decide which ordered state of Tables I and II represents best the stable configuration for dysprosium in zero external field. The only relevant data are those of Banister, Legvold, and Spedding (5), which give the lattice parameters a and c as functions of temperature. The parameter a decreases monotonically as the temperature decreases through the range in which dysprosium is antiferromagnetic, while the parameter c undergoes an anomalous expansion. Greenwald and Smart (32) have argued that it is reasonable to expect an anomalous expansion or contraction to occur in a direction which changes the distance between a certain set of parallel planes which have the property that all the angular momentum vectors on a given plane are aligned parallel to each other, while the angular momenta on adjacent planes are aligned antiparallel to each other. If we accept their arguments, we would predict that the antiferromagnetic structure of dysprosium is either A_x or A_z.

V. SOLUTIONS IN THE PRESENCE OF AN EXTERNAL MAGNETIC FIELD

A. Fundamental Equations for Two Sublattices

We discussed in Chapter IV the solutions of the molecular field equations (4.2) and (4.3) for the case of zero external field. One solution was ferromagnetic, with the angular momenta of all the sublattices parallel and of equal magnitude. The other solutions were antiferromagnetic. If we restrict ourselves to the case of eight sublattices, we find that for each of the antiferromagnetic solutions there are only two inequivalent angular momenta. These angular momenta can be placed, then, on two sublattices, instead of the original eight. We assume that in the presence of a magnetic field there still will be only two inequivalent angular momenta, and write Eqs. (4.2) in the form

$$\begin{aligned} (\lambda_1 - \alpha)\,\vec{S_1} - \beta\vec{S_2} - K\,S_{1z}\,\hat{z} &= \vec{H}\,, \\ -\beta\vec{S_1} + (\lambda_2 - \alpha)\,\vec{S_2} - K\,S_{2z}\,\hat{z} &= \vec{H}\,, \end{aligned} \tag{5.1}$$

where α and β are linear combinations of the coefficients p, q, and r. The atoms on the same sublattice now interact with a Weiss molecular field coefficient α, even though the original sublattices were chosen so that there was no self-interaction. This comes about because of the way we have combined several of the original sublattices to form the new sublattices.

For definiteness we take $K>0$, so that the states stable in zero field have their angular momenta aligned along the z axis. Furthermore, if states F_z and A_z are assumed to be the competing states in the ferromagnetic-antiferromagnetic transition, the field coefficients α and β are given by the relations

$$\alpha = (T_{Fz} + T_{Az} - 2C'K)/2C' = 3p/C'$$

$$\beta = (T_{Fz} - T_{Az})/2C' = (3q+r)/C' \quad , \qquad (5.2)$$

where T_{Fz} and T_{Az} are the critical temperatures given in Table I in terms of the field coefficients p, q, and r. The coefficient α is a ferromagnetic coupling, and the stable state with $H=0$ is F_z or A_z according as $\beta>0$ or $\beta<0$.

For convenience, take the field H always in the x-z plane, and with its x and z components greater than or equal to zero. Equations (5.1), written out in component form, are

$$(\lambda_1 - \alpha)\, S_{1x} - \beta\, S_{2x} = H_x \quad , \qquad (5.3a)$$

$$-\beta\, S_{1x} + (\lambda_2 - \alpha)\, S_{2x} = H_x \quad , \qquad (5.3b)$$

$$(\lambda_1 - \alpha)\, S_{1y} - \beta\, S_{2y} = 0 \quad , \qquad (5.3c)$$

$$-\beta\, S_{1y} + (\lambda_2 - \alpha)\, S_{2y} = 0 \quad , \qquad (5.3d)$$

$$(\lambda_1 - \alpha - K)\, S_{1z} - \beta\, S_{2z} = H_z \quad , \qquad (5.3e)$$

$$-\beta\, S_{1z} + (\lambda_2 - \alpha - K)\, S_{2z} = H_z \quad , \qquad (5.3f)$$

where the magnitudes S_i are given by

$$S_i = J\, B_J(\mu\lambda_i S_i/kT) \ . \qquad (5.4)$$

We first of all seek consistent solutions of Eqs. (5.3) and (5.4), and investigate later the question of the relative stability of the various solutions for given values of H and T.

Observe that Eqs. (5.3) and (5.4) comprise a set of simultaneous, transcendental equations. Instead of solving directly for S_1 and S_2 as functions of H and T, the following technique is effective. Assume values for λ_1 and λ_2, and then determine H_x and H_z so that the molecular field equations are satisfied. To proceed in this manner, we solve Eqs. (5.3a) and (5.3b) for S_{1x} and Eqs. (5.3e) and (5.3f) for S_{1z}, obtaining

$$S_{1x} = \left[H_x(\lambda_2 - \alpha + \beta)\right]/\Delta_x \ , \qquad (5.5)$$

$$S_{1z} = \left[H_z(\lambda_2 - \alpha + \beta - K)\right]/\Delta_z \ , \qquad (5.6)$$

where

$$\Delta_x = (\lambda_1 - \alpha)(\lambda_2 - \alpha) - \beta^2 \ , \qquad (5.7)$$

$$\Delta_z = (\lambda_1 - \alpha - K)(\lambda_2 - \alpha - K) - \beta^2 \ . \qquad (5.8)$$

We see from Eqs. (5.3c) and (5.3d) that unless Δ_x vanishes, the components S_{1y} and S_{2y} are zero. The special case when $\Delta_x = 0$ will be considered later. As long as S_{1y} and S_{2y}

vanish, H_x and H_z must satisfy the equation

$$S_{1x}^2 + S_{1z}^2 = S_1^2 \quad , \tag{5.9}$$

or

$$\left[(\lambda_2-\alpha+\beta)/\Delta_x\right]^2 H_x^2 + \left[(\lambda_2-\alpha+\beta-K)/\Delta_z\right]^2 H_z^2 = S_1^2 \quad . \tag{5.10}$$

We derive in similar fashion relations involving S_2, which are

$$S_{2x} = \left[H_x(\lambda_1 - \alpha + \beta)\right]/\Delta_x \quad , \tag{5.11}$$

$$S_{2z} = \left[H_z(\lambda_1 - a + \beta - K)\right]/\Delta_z \quad , \tag{5.12}$$

$$\left[(\lambda_1-\alpha+\beta)/\Delta_x\right]^2 H_x^2 + \left[(\lambda_1-\alpha+\beta-K)/\Delta_z\right]^2 H_z^2 = S_2^2 \quad . \tag{5.13}$$

Equations (5.10) and (5.13) are ellipses in the H_x-H_z plane. These ellipses are identical if λ_1 and λ_2 are equal. Otherwise they have a common solution or intersection if the ellipse with the larger H_x axis has the smaller H_z axis. The condition for this is that

$$\left(|\lambda_1-\alpha+\beta|S_1-|\lambda_2-\alpha+\beta|S_2\right) \times \left(|\lambda_1-\alpha+\beta-K|S_1-|\lambda_2-\alpha+\beta-K|S_2\right) \leq 0 \quad . \tag{5.14}$$

Condition (5.14) determines a region in λ_1-λ_2 space for which consistent solutions to Eqs. (5.3) and (5.4) exist. If we

solve Eqs. (5.10) and (5.13) for H_x^2 and H_z^2, we obtain

$$H_x^2 = \frac{\Delta_x^2 \left[(\lambda_1-\alpha+\beta-K)^2 S_1^2 - (\lambda_2-\alpha+\beta-K)^2 S_2^2\right]}{D} , \qquad (5.15)$$

$$H_z^2 = \frac{\Delta_z^2 \left[(\lambda_2-\alpha+\beta)^2 S_2^2 - (\lambda_1-\alpha+\beta)^2 S_1^2\right]}{D} , \qquad (5.16)$$

where

$$D = 2K(\lambda_1-\lambda_2)\left[(\lambda_1-\alpha+\beta-K/2)(\lambda_2-\alpha+\beta-K/2) - K^2/4\right] . \qquad (5.17)$$

Dividing Eq. (5.15) by Eq. (5.16), we find that

$$\tan^2\phi = \frac{\Delta_x^2 \left[(\lambda_1-\alpha+\beta-K)^2 S_1^2 - (\lambda_2-\alpha+\beta-K)^2 S_2^2\right]}{\Delta_z^2 \left[(\lambda_2-\alpha+\beta)^2 S_2^2 - (\lambda_1-\alpha+\beta)^2 S_1^2\right]} , \qquad (5.18)$$

where ϕ is the angle between $\vec{H}$ and the z axis. The ratio of S_{1x} to S_{1z} is obtained from Eqs. (5.5) and (5.6) as

$$\frac{S_{1x}}{S_{1z}} = \frac{\Delta_z(\lambda_2-\alpha+\beta)\tan\phi}{\Delta_x(\lambda_2-\alpha+\beta-K)} . \qquad (5.19)$$

Similarly, from Eqs. (5.11) and (5.12) we find that

$$\frac{S_{2x}}{S_{2z}} = \frac{\Delta_z(\lambda_1-\alpha+\beta)\tan\phi}{\Delta_x(\lambda_1-\alpha+\beta-K)} . \qquad (5.20)$$

We now have the necessary formulas for studying the nature of the solutions of the molecular field equations (5.3) and (5.4) for all directions and magnitudes of the external field $\vec{H}$ and for all ranges of temperature from

0°K to temperatures greater than the highest critical temperature.

B. Discussion of the Existence of Solutions

1. Compatibility conditions

Consistent solutions of the molecular field equations exist for values of λ_1 and λ_2 which satisfy condition (5.14). For examination of condition (5.14), it is useful to consider the curves in the λ_1-λ_2 plane determined by the equations

$$\left|\lambda_1-\alpha+\beta\right|S_1 = \left|\lambda_2-\alpha+\beta\right|S_2 \quad , \tag{5.21}$$

$$\left|\lambda_1-\alpha+\beta-K\right|S_1 = \left|\lambda_2-\alpha+\beta-K\right|S_2 \quad . \tag{5.22}$$

For the general case, the region in which the allowed values of λ_1 and λ_2 lie is bounded by curves (5.21) and (5.22). The nature of these curves changes with temperature and therefore the properties of the solutions of the molecular field equations are different in the different temperature ranges.

Let us consider as a function of λ_1 the expression

$$G_i = (\lambda_i-\rho)S_i \quad , \tag{5.23}$$

where S_i is given as a function of temperature by Eq. (5.4) and λ_i and S_i are both greater than or equal to zero. If the temperature T is such that

$$T \geq c\cdot\rho \quad , \tag{5.24}$$

then G_i is a monotonic function of λ_i, of the form shown in curve A of Fig. 4. The equation

$$|\lambda_1-\rho|\,S_1 = |\lambda_2-\rho|S_2 \tag{5.25}$$

has therefore only one solution, which is $\lambda_1=\lambda_2$. However, if

$$T < C'\rho \quad , \tag{5.26}$$

we observe that G_i is now a non-monotonic function of λ_i which has the value zero for the two roots

$$\lambda_i = T/C';\rho \quad . \tag{5.27}$$

The behavior of G_i for this case is shown by curve B of Fig. 4. Equation (5.25) now has, in addition to the usual solution $\lambda_1 = \lambda_2$, another solution for which $\lambda_1 \neq \lambda_2$. These values of λ_1 and λ_2 lie on a closed curve in the λ_1-λ_2 plane, an example of which is shown in Fig. 5.

We now proceed to discuss the behavior of the solutions of the molecular field equations for the various significant temperature ranges.

2. Solutions for $T>C'(\alpha-\beta+K)$

For temperatures such that $T>C'(\alpha-\beta+K)$, observe that Eqs. (5.21) and (5.22) have but one solution, $\lambda_1=\lambda_2$, because the functions $(\lambda_i-\alpha+\beta)S_i$ and $(\lambda_i-\alpha+\beta-K)S_i$ are both monotonic functions of λ_i. For this range of temperature, the solution of Eqs. (5.3) has the property that $\overrightarrow{S_1} = \overrightarrow{S_2}$.

Fig. 4. Qualitative behavior for different temperatures of G_i as a function of λ_i, where the function G_i is defined in Eq. (5.23). The dashed straight line is the asymptote approached by F_i for large λ_i.

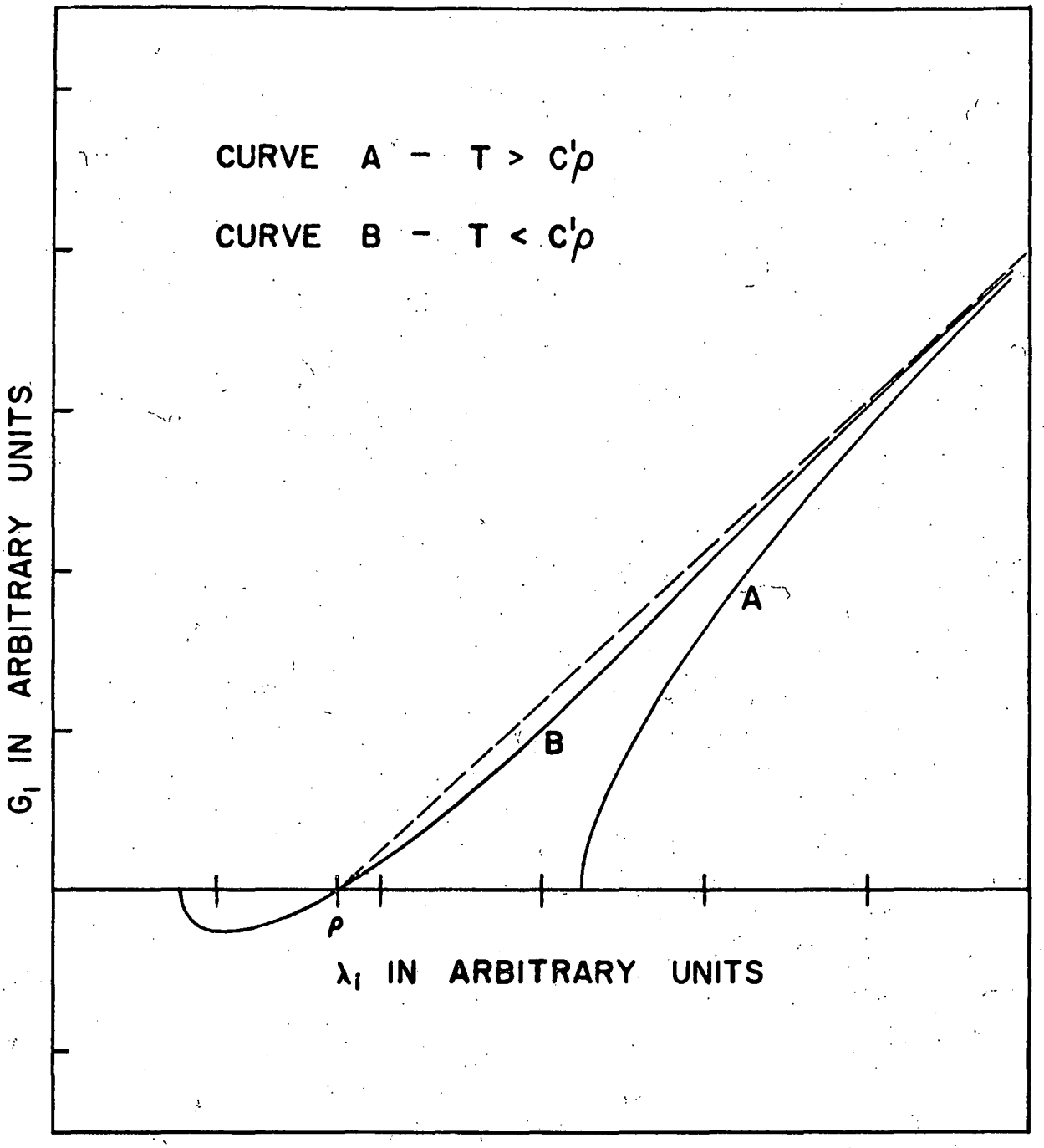
CURVE A - T > C'ρ
CURVE B - T < C'ρ
G_I IN ARBITRARY UNITS
A
B
ρ
λ_I IN ARBITRARY UNITS

Fig. 5. The λ-diagram for $T<C'\rho$. The closed curve is obtained from Eq. (5.25). The region inside the closed curve contains λ's for which consistent solutions of the molecular field equations exist, when $\rho = \alpha - \beta + K$ and $T>C'(\alpha - \beta)$.

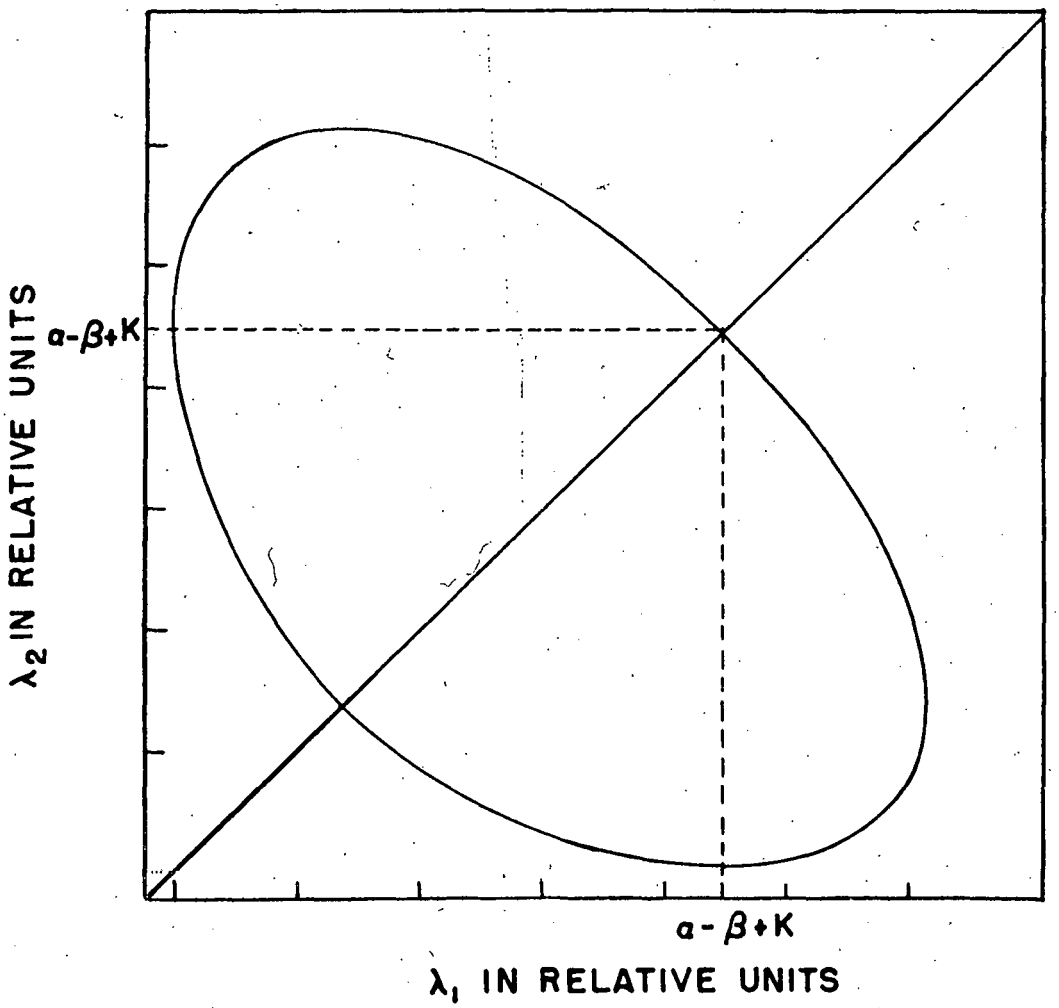
α-β+K
λ2 IN RELATIVE UNITS
α-β+K
λ1 IN RELATIVE UNITS

This solution applies for the range of temperatures in which the system is paramagnetic, that is, when T is greater than the highest critical temperature. The zero field susceptibility for this case can be derived most easily from consideration of Eqs. (3.20) and (5.3). For sufficiently high temperatures, Eq. (3.20) can be written in the approximate form

$$S_i = C' H_i/T \ , \tag{5.28}$$

so that from Eq. (4.1)

$$\lambda_i = T/C' \ . \tag{5.29}$$

From Eqs. (5.3a), (5.3b), (5.3e), and (5.3f) we obtain

$$S_{1x} = S_{2x} = C' H_x/(T-T_{Fx}) \ , \tag{5.30}$$

$$S_{1z} = S_{2z} = C' H_z/(T-T_{Fz}) \ , \tag{5.31}$$

where

$$T_{Fz} = C' (\alpha+\beta+K) \ , \tag{5.32}$$

$$T_{Fx} = C' (\alpha+\beta) \ , \tag{5.33}$$

and α and β are given in Eq. (5.2). If for purposes of comparison with experiment we take the component of the magnetization in the direction of the field, we find

$$M = C \left[(\sin^2\phi)/(T-T_{Fx}) \pm (\cos^2\phi)/(T-T_{Fz})\right] H \ , \tag{5.34}$$

where ϕ is the angle between $\vec{H}$ and the z axis, and C is the Curie constant given by $C = 2nN(g_J\mu_B)^2J(J+1)/3k$. For a polycrystalline sample in which all the crystallites are randomly oriented, the susceptibility χ is given by

$$\chi = \frac{C(3T - T_{Fz} - 2T_{Fx})}{3(T - T_{Fx})(T - T_{Fz})} , \qquad (5.35)$$

which is obtained by averaging M in Eq. (5.34) over all values of ϕ and dividing by H.

3. Solutions for $C'(\alpha-\beta) < T < C'(\alpha-\beta+K)$

The situation for this temperature range is as follows. Equation (5.21) still has only one solution, $\lambda_1=\lambda_2$, since the function $|\lambda_1-\alpha+\beta|S_1$ is still monotonic. However, since $|\lambda_1-\alpha+\beta-K|S_1$ is now non-monotonic, Eq. (5.22) has two kinds of solutions. We find as usual that $\lambda_1=\lambda_2$ is a solution, but now a second solution is possible for which $\lambda_1\neq\lambda_2$. The curve defined by Eq. (5.22) is shown - for a typical case for this temperature range - in Fig. 5. Examination of Eqs. (5.10) and (5.13) reveals that the allowed region in λ-space is the region inside the closed curve defined by Eq. (5.22). The line $(\lambda_1=\lambda_2)$ also contains λ's for which the equations are consistent. It follows from Eq. (5.18) that $\vec{H}$ is directed along the z axis ($\phi=0$) for λ's on the boundary line of the allowed region.

4. Solutions for $T<C'(\alpha-\beta)$

In this final temperature range to be considered, the functions $|\lambda_i-\alpha+\beta|S_i$ and $|\lambda_i-\alpha+\beta-K|S_i$ are both non-monotonic functions of λ_i, so that in addition to the usual solution ($\lambda_1=\lambda_2$), both Eqs. (5.21) and (5.22) have solutions for which $\lambda_1\neq\lambda_2$. Inspection of Eqs. (5.10) and (5.13) reveals that for this case the allowed region is bounded by the curves (5.21) and (5.22), and again values of the λ's on the line ($\lambda_1=\lambda_2$) are allowed. The "λ-diagram" for this case will be discussed in detail later in this chapter, since this case is of considerable physical interest.

C. The State F

For the case $\lambda_1=\lambda_2$, Eqs. (5.3) and (5.4) show that $\vec{S}_1=\vec{S}_2$. The two ellipses, Eqs. (5.10) and (5.13), both reduce to the single relation

$$(\lambda-\alpha-\beta)^{-2}H_x^2 + (\lambda-\alpha-\beta-K)^{-2}H_z^2 = S^2 \quad . \qquad (5.36)$$

Equations (5.4) and (5.36) express λ as a transcendental function of H_x, H_z, and T. Since we have from Eqs. (5.5), (5.6), (5.11), and (5.12) that

$$\frac{S_{1x}}{S_{1z}} = \frac{S_{2x}}{S_{2z}} = \frac{\Delta_z(\lambda-\alpha+\beta)\tan\phi}{\Delta_x(\lambda-\alpha+\beta-K)} \quad , \qquad (5.37)$$

Eqs. (5.4), (5.36) and (5.37) determine completely this state.

Because the sublattice magnetizations are equal and parallel for this ordered arrangement, we refer to it as ferromagnetic state F, even though it may be the stable state only in the presence of large applied magnetic fields for temperatures above the F-A transition. Gorter and Haantjes (27) use the term paramagnetic saturation to refer to the state which we call F, when for large fields it is stable relative to the antiferromagnetic state.

D. The State A_x

There exists a type of solution of the molecular field equations for which $\vec{S_1}$ and $\vec{S_2}$ lie outside the x-z plane. For this solution to exist, the determinant Δ_x must vanish, so that

$$\Delta_x = (\lambda_1-\alpha)(\lambda_2-\alpha) - \beta^2 = 0 \quad . \tag{5.38}$$

When $H_x \neq 0$, it follows from Eqs. (5.3a) and (5.3b) for the x components that

$$\lambda_1 = \lambda_2 = \alpha - \beta \quad . \tag{5.39}$$

For this value of λ_1 and λ_2, the solution of Eqs. (5.3) is

$$\begin{aligned} S_{1x} &= S_{2x} = H_x/(-2\beta) \quad , \\ S_{1y} &= - S_{2y} \quad , \\ S_{1z} &= S_{2z} = H_z/(-2\beta-K), \end{aligned} \tag{5.40}$$

Fig. 6. Schematic representation of the angular momenta for state A_x, when K>0 and the magnetic field H is less than the critical value given by Eq. (5.42).

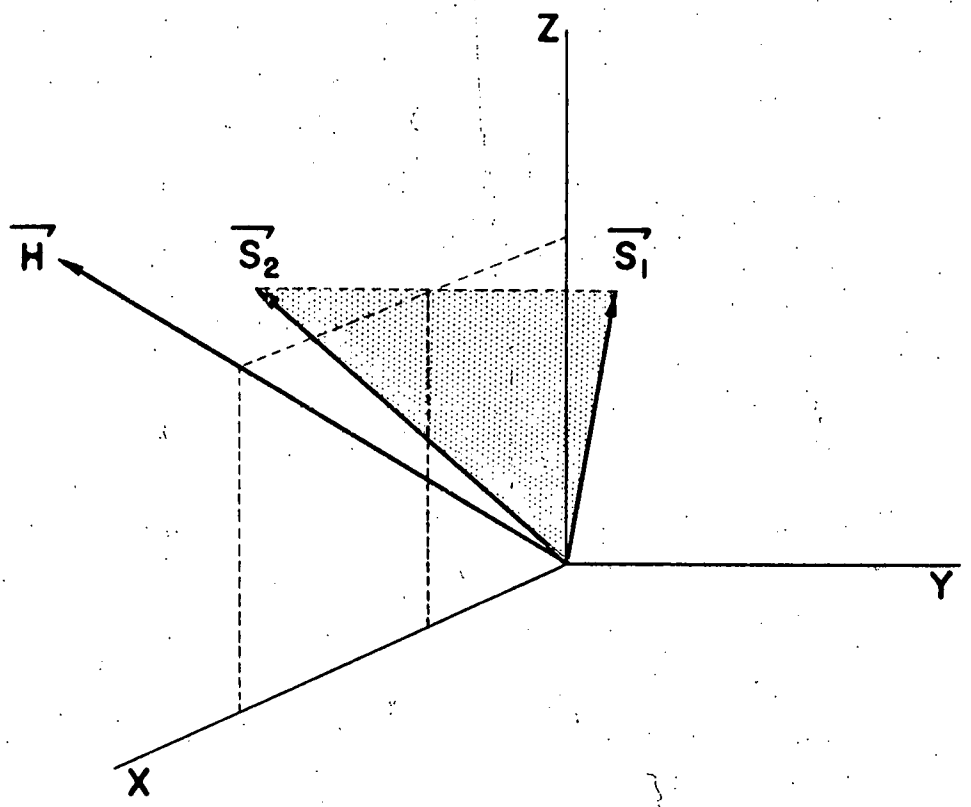
Z
$\overrightarrow{H}$
$\overrightarrow{S_2}$
$\overrightarrow{S_1}$
Y
X

and S_1 and S_2 are known as functions of T from Eq. (5.4). If we set $S_1=S_2=S$, the y components of $\vec{S_1}$ and $\vec{S_2}$ are given by the relation

$$S_{1y} = - S_{2y} = \left[S^2-(H_x/2\beta)^2-H_z^2/(2\beta+K)^2\right]^{\frac{1}{2}} . \qquad (5.41)$$

It is apparent from Eq. (5.41) that if the magnetic field exceeds a certain critical value $\vec{H_c}$, which depends upon the angle ϕ, this antiferromagnetic state cannot exist. The critical field curve, obtained from Eq. (5.41) by setting $S_{1y} = S_{2y} = 0$, is

$$(H_{cx}/2\beta)^2 + H_{cz}^2/(2\beta+K)^2 = S^2 . \qquad (5.42)$$

This curve is an ellipse in the H_x - H_z plane. For values of the magnetic field which lie on the ellipse, the antiferromagnetic state described here and the state F discussed above are identical. For H=0, this antiferromagnetic state is identical with state A_x described in Chapter IV. Therefore, we also designate this state by the symbol A_x when a magnetic field is present. The arrangement of angular momenta for state A_x is shown in Fig. 6, for a case where H is less than the critical field and K>0.

As H increases, $\vec{S_1}$ and $\vec{S_2}$ become more nearly parallel to each other, until they become parallel at the critical field H_c given in Eq. (5.42). The total magnetization M_{Ax} of a single crystal in state A_x is

$$M_{Ax} = 2nNg_J\mu_B(S_{1x}^2 + S_{1z}^2)^{\frac{1}{2}}$$

$$= 2nNg_J\mu_B\left[(H_x/2\beta)^2 + H_z^2/(2\beta+K)^2\right]^{\frac{1}{2}} . \qquad (5.43)$$

Because of the anisotropy, the total magnetization vector is not quite parallel to the applied field $\vec{H}$. For a given direction of $\vec{H}$ however, M_{Ax} is a linear function of H and the susceptibility is constant.

E. The State A_z

There still remains one type of solution of the molecular field equations which as yet we have not discussed. This is the solution which, in the limit as H approaches zero, becomes identical with the state A_z described in Chapter IV. We call this solution state A_z for all magnitudes and directions of the applied magnetic field for which it exists. In order to investigate the properties of state A_z and at the same time anticipate some of the results needed later for the discussion of the properties of dysprosium, we consider the following case. We assume that $K>0$ and that $\beta<0$, so that state A_z is the stable state for $H=0$ and the preferred axis is the z axis. We take $T<C'(\alpha+\beta+K)$, so that state A_z and F_z are both stable relative to the disordered state, and for this temperature range explore in detail the significance of the various possible (compatible) values of λ_1 and λ_2 and the corresponding sublattice angular momenta.

Figure 7 shows a typical "λ-diagram" or plot of the

Fig. 7. Typical λ-diagram showing values of λ_1 and λ_2 for which consistent solutions of the molecular field equations exist when $T<C'(\alpha+\beta+K)$, so that states A and F are both stable relative to the disordered state. The region of allowed λ's is bounded by the two closed curves. The line ($\lambda_1=\lambda_2$) also contains allowed values of the λ's. This diagram and Figs. 8 through 11 were calculated for J=15/2 and for a temperature of 143.6°K, using the values of the parameters given in Table IV.

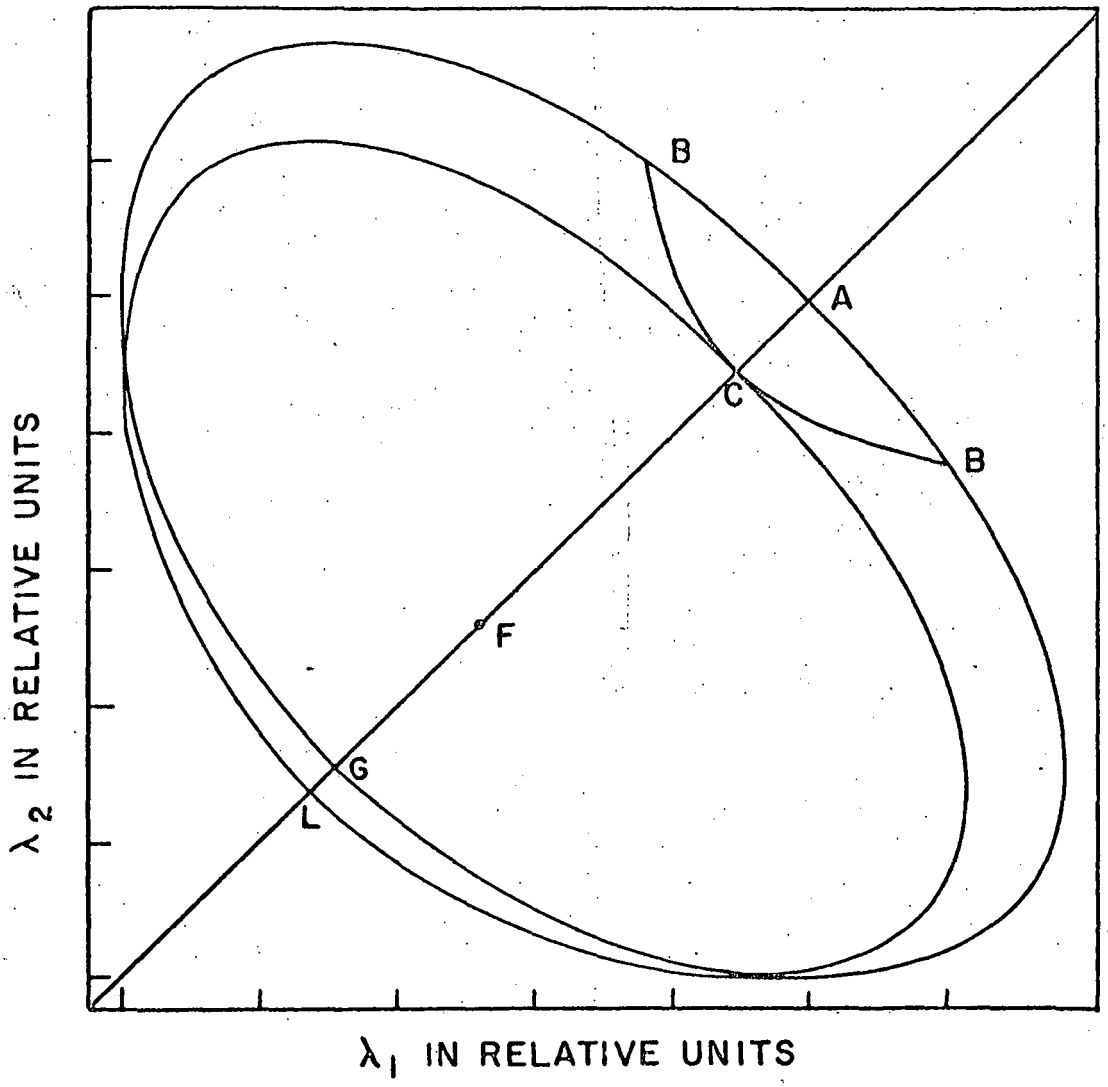
B
A
C
B
F
G
L
λ_2 IN RELATIVE UNITS
λ_1 IN RELATIVE UNITS

Fig. 8. The stable region of the λ-diagram of Fig. 7.

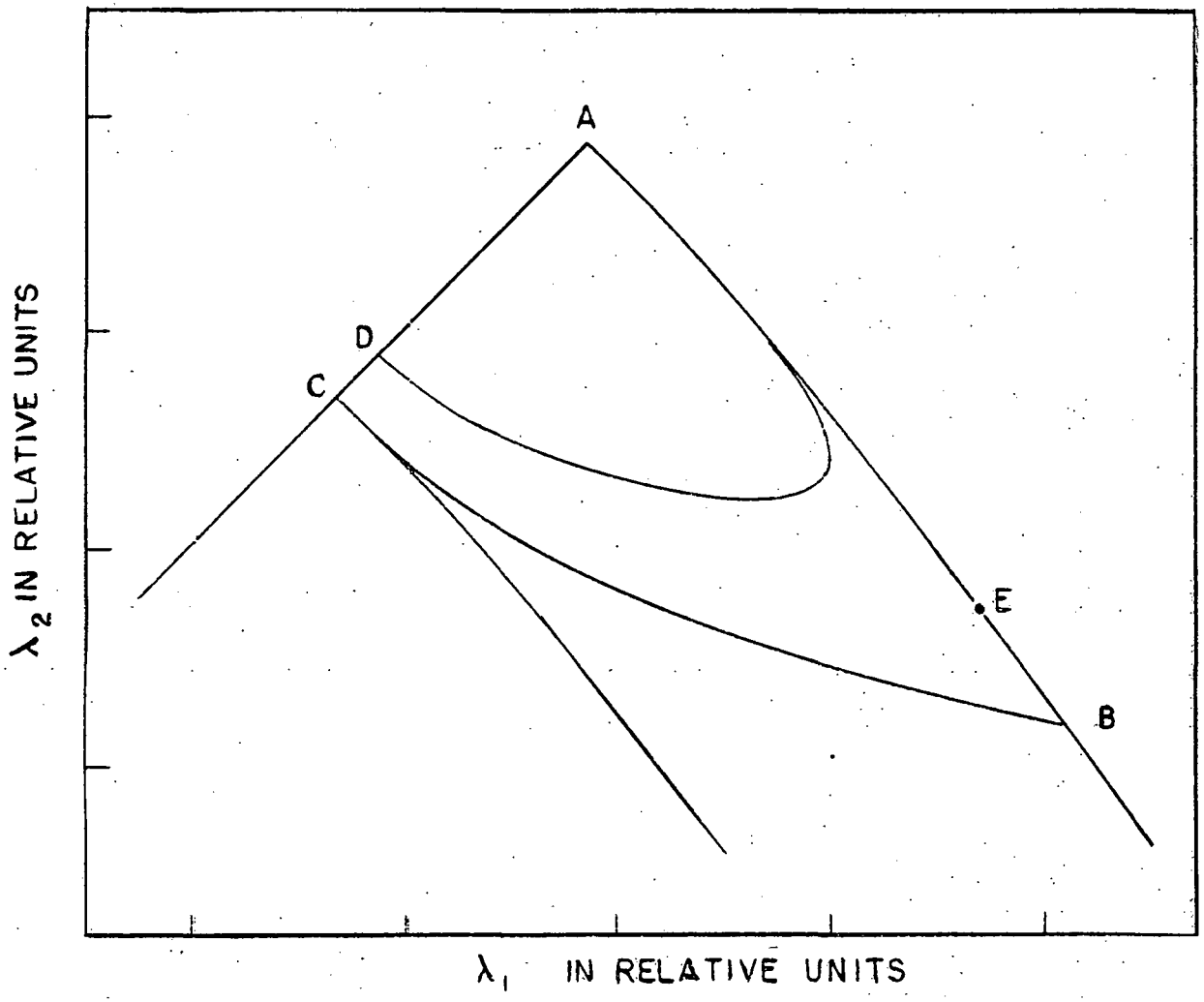
A
D
C
E
B
λ_2 IN RELATIVE UNITS
λ_1 IN RELATIVE UNITS

important regions in the space of λ_1 and λ_2 for this temperature range. The region of allowed λ's lies between the two closed curves or along the line ($\lambda_1=\lambda_2$). The point A represents state A_z, point F represents state F, and point C represents state A_x for H = 0. The curve connecting points A, B, and G is obtained from Eq. (5.22) and contain λ's for which $\phi=0$. The curve connecting points B and C is the curve $\Delta_x=0$, which from Eq. (5.18) also contains states for which $\phi=0$. The curve connecting points C and L comes from Eq. (5.21) and contains λ's for which $\phi=90°$.

An exploration of the λ-diagram for particular cases has revealed that for a given $\vec{H}$ and T there can be more than one state for which molecular field equations (5.3) and (5.4) are satisfied. However, in all cases, the state having the lowest free energy lies in the area bounded by the curves connecting the points A, B, and C. This area is the area of physical interest, and we will concentrate our attention on it. The area ABC is shown in more detail in Fig. 8.

For H=0, state A_z is the stable state and it is located at point A (where $\lambda_1=\lambda_2=\alpha-\beta+K$) in Fig. 8. The behavior of state A_z as the magnetic field increases in magnitude depends upon the direction of the field relative to the preferred axis. A discussion of the behavior of state A_z for small magnetic fields - for λ's in the immediate neighborhood of point A, which is a rather singular point - is given in Appendix C. The behavior for large magnetic fields is

discussed below for the two special cases of $\phi=0$ and $\phi=90°$ before investigating the general case.

F. External Magnetic Field Parallel to the Z Axis

We now discuss the interesting case of H directed along the z axis, so that $\phi=0$. We will show that as the magnitude of the field increases for the range of temperature in which state A_z is stable for zero field, the system remains in state A_z until the threshold field for "spin flop" is reached. At this value of the field, the system changes discontinuously from state A_z to A_x. As the field increases still further, state A_x is deformed continuously into state F.

In Fig. 8, the curves AEB and BC contain all points for which $\phi=0$. As state A_z moves down the curve AEB toward point B, the magnitude of H, given by Eq. (5.16) increases. As state A_z moves along the curve BC from B to C, H decreases. For a certain range of values of H then, there are two different solutions of the equations. We have to appeal to free energy (3.21) to decide which is stable. For the present case where the structure is subdivided into two sublattices, the free energy (3.21) can be written

$$F = (n/2)\left[(F_1 + F_2) - Ng_J\mu_B \vec{H}.(\vec{S_1} + \vec{S_2})\right] , \quad (5.44)$$

with

$$F_1 = Ng_J\mu_B\lambda_1 S_1^2 - kT \ln Z\ (\mu\lambda_1 S_1/kT) , \quad (5.45)$$

62

Fig. 9. The free energies of states A_x and A_z as functions of H, the magnitude of the applied magnetic field, for H directed along the z axis.

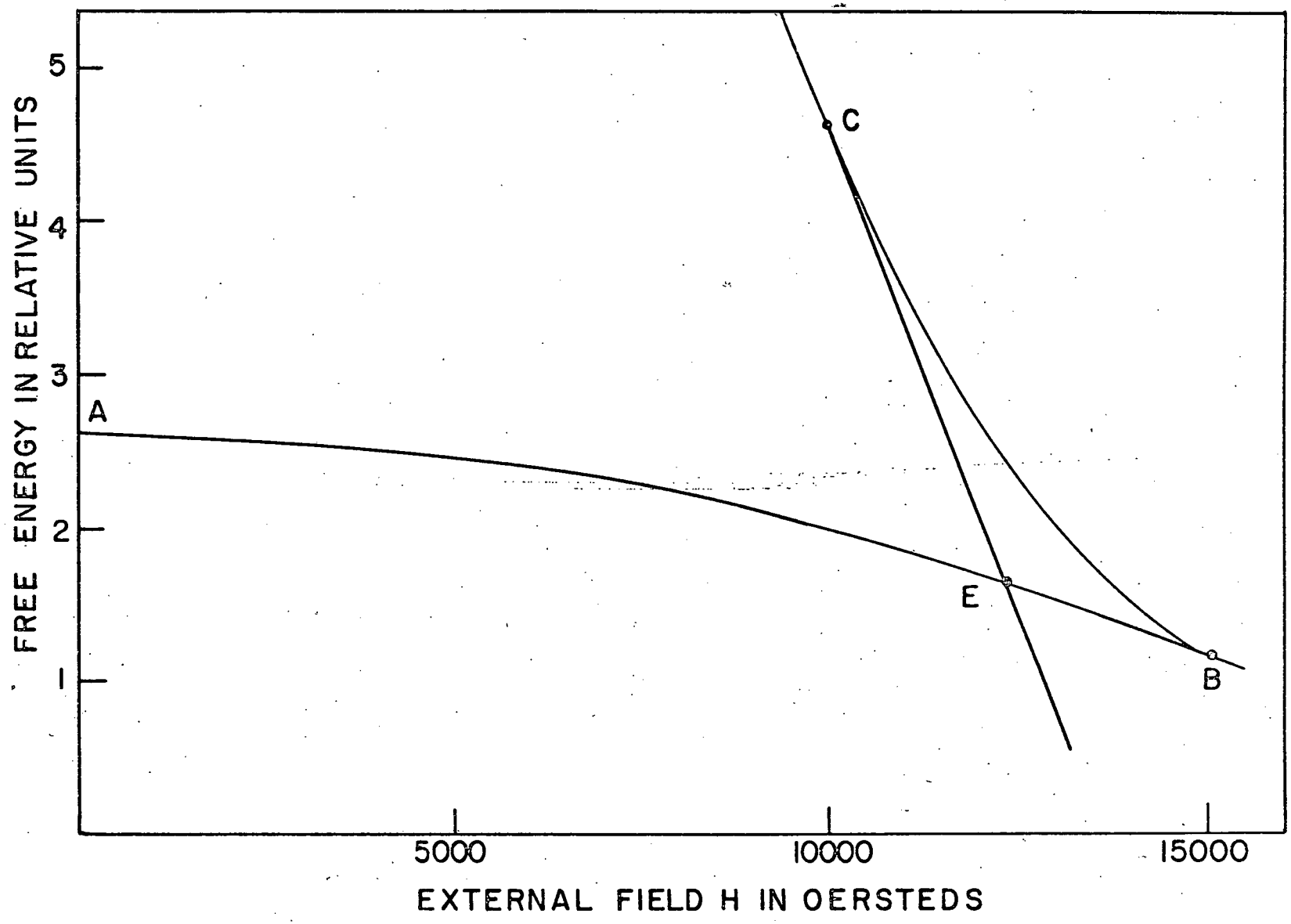
FREE ENERGY IN RELATIVE UNITS
5
4
3
2
1
A
C
E
B
5000
10000
15000
EXTERNAL FIELD H IN OERSTEDS

$$F_2 = Ng_J\mu_B\lambda_2 S_2^2 - kT \ln Z\,(\mu\lambda_2 S_2/kT) \quad . \qquad (5.46)$$

Here the magnitudes S_1 and S_2 are obtained from Eq. (5.4) with λ_i equal to λ_1 and λ_2, respectively. The function $Z(\mu\lambda_i S_i/kT)$ is given by Eq. (3.16) with $y_i=\mu\lambda_i S_i/kT$.

In Fig. 9 are shown free energies calculated from Eq. (5.44) for magnetic fields given by points on the lines AEB and BC, respectively. The points A, B, C, and E correspond to the same states as in Fig. 8. We see in Fig. 9 that states on the curve BC are unstable relative to those on AEB for the same values of H.

We have already shown that for magnitudes of H less than a critical value obtained from Eq. (5.42) for $H_x=0$, state A_x (corresponding to point C of Fig. 8) is also a solution of the molecular field equations. For state A_x, we have $\lambda_1=\lambda_2=\alpha-\beta$, so that the free energy F_{Ax} for $H_x=0$ is

$$F_{Ax} = F_{Ax}^{\circ} - (\tfrac{1}{2})\chi_{Ax}H_z^2 \quad , \qquad (5.47)$$

where F_{Ax}° is the function F_1 of Eq. (5.45) with $\lambda_1=\alpha-\beta$, S_{Ax} is the solution of Eq. (5.4) with $\lambda_1=\alpha-\beta$, and

$$\chi_{Ax} = -\,2nNg_J\mu_B/(2\beta+K) \quad . \qquad (5.48)$$

The susceptibility χ_{Ax} is obtained from Eq. (5.43) with $H_x=0$ from the definition

$$\chi_{Ax} = M_{Ax}/H_z = -\,2nNg_J\mu_B/(2\beta+K). \qquad (5.49$$

Since F_{Ax}° is independent of H, free energy F_{Ax} is a

quadratic function of H_z for $\phi=0$. The free energy F_{Ax} is given as a function of H by curve CE in Fig. 9.

For H=0, state A_z is stable and located at point A in Fig. 9. As the applied field increases, the free energy of state A_z drops slowly because the susceptibility of state A_z for $\phi=0$ is relatively low. State A_x has a much higher free energy at low fields, which drops very rapidly as the external field increases because state A_x has a relatively large susceptibility. As shown in Fig. 9, the free energies for states A_x and A_z cross when the magnetic field reaches the value at point E and the phenomenon of "spin flop" occurs. In "spin flop", the stable state changes from state A_z to A_x and the direction of alignment of the $\vec{S_i}$ switches suddenly from parallel to the z axis into a direction with a component perpendicular to the z axis. The phenomenon of "spin flop" has been observed experimentally in $CuCl_2.2H_2O$ by means of proton resonance. An extensive review of the subject is given by Nagamiya, Yosida, and Kubo (15).

In order to continue the discussion of the behavior of our model, and in particular, to develop an approximate formula for the temperature variation of the threshold field for spin flop, we need to have an expression for $\chi_{\parallel}$, the susceptibility in the limit of small fields directed along the preferred z axis of the system. For H directed along the z axis with a magnitude small enough so that the system

remains in state A_z, the susceptibility can be calculated by a method similar to that used by Van Vleck (17) and many others. Vectors $\vec{S_1}$, $\vec{S_2}$, and $\vec{H}$ have only z components, and the molecular field equations can be written

$$S_{1z} = J\, B_J(\mu H_1/kT) \quad , \tag{5.50}$$

$$S_{2z} = J\, B_J(\mu H_2/kT) \quad , \tag{5.51}$$

with the effective fields H_1 and H_2 given by

$$H_1 = H_z + \alpha\, S_{1z} + \beta\, S_{2z} \quad , \tag{5.52}$$

$$H_2 = H_z + \beta\, S_{1z} + \alpha\, S_{2z} \quad . \tag{5.53}$$

Since the system is in state A_z for applied fields small compared to the exchange interactions, vectors $\vec{S_1}$ and $\vec{S_2}$ are antiparallel to each other. Therefore, we have

$$H_1 = H_z + \alpha|S_{1z}| - \beta|S_{2z}| \quad , \tag{5.54}$$

$$H_2 = H_z + \beta|S_{1z}| - \alpha|S_{2z}| \quad . \tag{5.55}$$

To compute $\chi_{\parallel}$, the susceptibility parallel to the z axis, which is defined by the equation

$$\chi_{\parallel} = \lim_{H \to 0} nNg_J\mu_B\,(dS_1/dH + dS_2/dH) \quad , \tag{5.56}$$

take the derivatives of Eqs. (5.50) and (5.51) with respect to H and use Eqs. (5.54) and (5.55) for the effective fields. After solving the resulting two simultaneous equations for

dS_1/dH and dS_2/dH, taking their sum, and setting H=0, we obtain

$$\chi_{\parallel} = \frac{2nN(\mu^2/k)\ B_J'(\mu H_o/kT)}{T - 3J(J+1)^{-1}T_{Fz}B_J'(\mu H_o/kT)} \quad , \qquad (5.57)$$

with $\mu = g\mu_B J$; B_J' signifies the derivative of B_J with respect to its argument. The temperature T_{Fz} is the critical temperature for state F_z, defined by

$$T_{Fz'} = C' \ (\alpha+\beta+K) \quad , \qquad (5.58)$$

and H_o is the value of H_1 or H_2 when the applied field H is zero. This is the familiar formula for $\chi_{\parallel}$ given by Van Vleck (17), Anderson (18), and many others.

For the free energy of state A_z, a good approximation can be obtained as follows. From statistical mechanics, we have that

$$M = - (\partial F/\partial H)_T \quad , \qquad (5.59)$$

where F is the free energy and M is the magnetization. We also have

$$\chi_{\parallel} = - \lim_{H\to 0} \partial^2 F/\partial H^2 \quad . \qquad (5.60)$$

The expansion of the free energy for state A_z in the presence of a field is therefore, to order H^2,

$$F_{Az} \simeq F_{Az}^{\circ} - \tfrac{1}{2}\chi_{\parallel}H^2 \quad , \qquad (5.61)$$

where F_{Az}° is the free energy for state A_z in zero field. The linear term in the expansion is missing because the magnetization is zero for antiferromagnetic state A_z when H=0. Approximation (5.61) is quite good when H is small compared to the molecular fields arising from the exchange interactions.

A useful approximation for the temperature variation of the threshold field for spin flop can be obtained in a similar way. This approximation is valid when the anisotropy energy is small enough so that spin flop occurs at a field which is small compared to the exchange interactions. The spin flop occurs at the magnetic field strength H_f for which the free energies F_{Ax} and F_{Az} become equal. Using Eqs. (5.61) and (5.47) for the two free energies, we determine H_f from the equation

$$F_{Az}^{\circ} - (\tfrac{1}{2})\chi_{\parallel}H_f^2 = F_{Ax}^{\circ} - (\tfrac{1}{2})\chi_{Ax}H_f^2 \quad , \qquad (5.62)$$

where χ_{Ax} is given by Eq. (5.48). It follows from Eq. (5.62) that

$$H_f = \left[2(F_{Ax}^{\circ} - F_{Az}^{\circ})/(\chi_{Ax} - \chi_{\parallel})\right]^{\frac{1}{2}} \quad . \qquad (5.63)$$

When the anisotropy coefficient K is small, the difference $(F_{Ax}^{\circ} - F_{Az}^{\circ})$ can be expanded in a power series in K in the following manner. The free energy F for H=0 can be written as a function of λ in the form

$$F(\lambda) = nNg_J\mu_B\lambda S^2 - nkT \ln Z\left[g_J\mu_B\lambda S/kT\right] \quad , \qquad (5.64)$$

which is obtained by setting H=0 and $\lambda_1=\lambda_2=\lambda$ in Eq. (5.44), Z is given by Eq. (3.16), and S is obtained from Eq. (5.4) when λ_i is taken equal to λ.

From Eq. (5.64), we find

$$d\,F(\lambda)/d\lambda = -\,nNg_J\mu_B S^2 \quad . \tag{5.65}$$

The expansion of $F(\lambda)$ about the point $\lambda=\lambda_{Az}$, to the first order in $(\lambda-\lambda_{Az})$, is

$$F(\lambda) \simeq F_{Az}^{\circ} - nNg_J\mu_B(\lambda - \lambda_{Az})\left[S(\lambda_{Az})\right]^2 \quad , \tag{5.66}$$

where $F(\lambda_{Az})=F_{Az}^{\circ}$. Since $\lambda_{Az}-\lambda_{Ax}=K$, we have

$$F_{Ax}^{\circ} \simeq F_{Az}^{\circ} + nNg_J\mu_B KS^2 \quad , \tag{5.67}$$

and

$$F_{Ax}^{\circ} - F_{Az}^{\circ} \simeq nNg_J\mu_B KS^2 \quad . \tag{5.68}$$

Equation (5.63) therefore can be further approximated by

$$H_f \simeq \left[2nNg_J\mu_B KS^2/(\chi_{Ax} - \chi_{\parallel})\right]^{\frac{1}{2}} \quad . \tag{5.69}$$

Approximation (5.69) for the threshold field H_f is identical with the expression obtained earlier by Poulis and Hardemann (29), who assume, to first approximation, that the effect of the anisotropy on the exchange energy can be neglected.

For applied fields greater than H_f, the threshold field for spin flop, the system is in state A_x and exhibits the rather large constant susceptibility of Eq. (5.48). As the

Fig. 10. The magnetization as a function of H for ϕ = 0, 30, and 90° and T = 143.6°K.

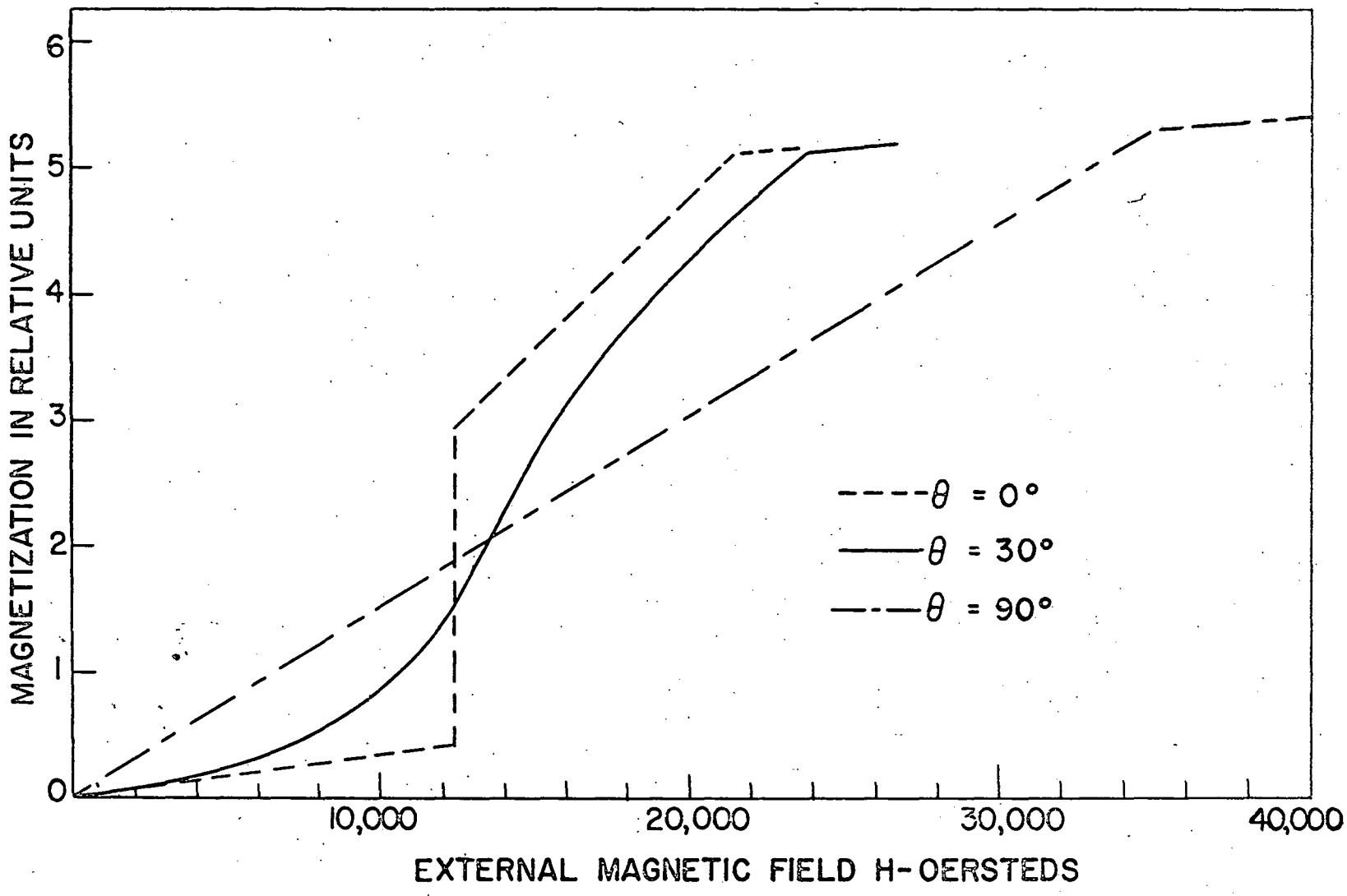
MAGNETIZATION IN RELATIVE UNITS
0
1
2
3
4
5
6
10,000
20,000
30,000
40,000
EXTERNAL MAGNETIC FIELD H-OERSTEDS
θ = 0°
θ = 30°
θ = 90°

field H increases, angular momenta $\vec{S}_1$ and $\vec{S}_2$ become more and more nearly parallel, and finally at the critical field H_c given by setting $H_x=0$ in Eq. (5.42), state A_x becomes identical with state F. Henceforward, we shall use the symbol H_c to refer to that value of the field strength for which an antiferromagnetic arrangement and state F have the same free energies. For field strengths higher than the value H_c, the system remains in state F. The typical behavior of the magnetization of the system for $\phi=0$ is given by the dashed curve in Fig. 10. There are three different susceptibilities for the system, when it is successively in states A_z, A_x, and F. The measurement of the susceptibility of a single crystal, therefore, should yield interesting information concerning the anisotropy energy of the crystal, as well as determining conclusively the axis of alignment of the angular momenta in zero field.

G. External Magnetic Field Perpendicular to the Z Axis

The behavior of our model for $\vec{H}$ directed perpendicular to the z axis, $\phi=90°$, is rather unspectacular. The system stays in state A_z up to the critical field H_c, where it becomes identical with state F. The representative point in the λ-diagram of Fig. 8 remains at point A for fields less than H_c. The momenta $\vec{S}_1$ and $\vec{S}_2$ remain constant in magnitude, but continuously change directions from their original orientation in which they were antiparallel to each other

and aligned along the z axis to their new arrangement in which they are parallel to each other and pointing along the x axis, parallel to the applied field. The representative point for state F moves up the line ($\lambda_1=\lambda_2$), as the external field increases, reaching point A when the field becomes equal to the value H_c.

To demonstrate these properties, we return to Eqs. (5.3) and (5.4). For $\phi=90°$, Eqs. (5.3e) and (5.3f) for the z components are homogeneous and have a non-trivial solution only if $\Delta_z=0$, where Δ_z is defined in Eq. (5.8). But the only point on the curve ($\Delta_z=0$) which lies in the allowed region of the λ-diagram of Fig. 8 is the point A, for which $\lambda_1=\lambda_2=\alpha-\beta+K$. Therefore, the λ's have the fixed value ($\alpha-\beta+K$) and from the z equations (5.3e) and (5.3f) we have

$$S_{1z} = - S_{2z} \quad . \tag{5.70}$$

Solving the x equations (5.3a) and (5.3b), we obtain

$$S_{1x} = S_{2x} = H_x/(-2\beta+K) \quad . \tag{5.71}$$

Since the magnitudes S_1 and S_2 are given by Eq. (5.4), we have

$$S_{1z} = - S_{2z} = \left[S_1^2 - H_x^2/(2\beta-K)^2\right]^{\frac{1}{2}} \quad . \tag{5.72}$$

From Eq. (5.72), we see that the critical field H_c for this state is given by

$$H_c = (-2\beta+K)\, S_1 \quad , \tag{5.73}$$

which is obtained by setting $S_{1z}=S_{2z}$ in Eq. (5.72). From Eq. (5.71), the susceptibility $\chi_\perp$, defined as the susceptibility for the magnetic field oriented perpendicular to the preferred z axis, is given by

$$\chi_\perp = 2nNg_J\mu_B/(-2\beta+K) \quad . \tag{5.74}$$

Using the definitions of the critical temperatures T_{Az} and T_{Fz} given by relations (5.2), we write Eq. (5.74) in the useful form

$$\chi_\perp = C/(T_{Az} - T_{Fz} + T_K) \quad , \tag{5.75}$$

where T_K, given by

$$T_K = C' K \quad , \tag{5.76}$$

is the anisotropy coefficient K expressed in units of the temperature. The susceptibility $\chi_\perp$ plays an important role in the interpretation of the experimental data for dysprosium, as will be described later.

The critical field H_c, given by Eq. (5.73), is the field at which states A_z and F become identical. Above H_c, the system remains in state F. The magnetization for $\phi=90°$ is given by the dot-dash curve of Fig. 10, where below the critical field H_c the susceptibility is constant, its value being given by Eq. (5.75).

H. External Magnetic Field in a General Direction

Finally, we describe the behavior of our model when $\vec{H}$ is neither parallel nor perpendicular to the z axis. The curve connecting points A and D in Fig. 8, while drawn for the case of $\phi=30°$, is typical of the curves for all ϕ's except those very near zero. As before, the stable state A_z starts out for zero field at point A and as the magnitude of the applied field increases the state proceeds toward D along the curve connecting points A and D. The magnetic field continues to increase all the way to point D. The magnitudes of $\vec{S_1}$ and $\vec{S_2}$ change, and their directions gradually become parallel. The critical field H_c is reached when state A_z reaches point D, which lies on the line $(\lambda_1=\lambda_2)$. State F, in the meanwhile, has been moving up the line $(\lambda_1=\lambda_2)$ as the magnitude of the field increases and arrives at D when $H = H_c$. As before, the critical field H_c is the field for which antiferromagnetic state A_z and state F become identical. State A_z is deformed continuously into state F as H increases. We show in Fig. 11 a schematic representation of the behavior of the S_i as H increases. Behavior similar to that shown in Fig. 11 has been described by Gorter and Haantjes (27) for a system at absolute zero. In Fig. 10, the magnetization for $\phi=30°$ is shown as a function of H by the solid curve.

Above H_c, only state F can exist. An expression for the critical field H_c as a function of ϕ can be derived by taking the limits of Eqs. (5.15), (5.16), and (5.18) as λ_1

Fig. 11. Schematic representation of the behavior of angular momenta $\vec{S}_1$ and $\vec{S}_2$ as the applied magnetic field, which makes an angle of 30° with the z axis, increases from zero to very large values.

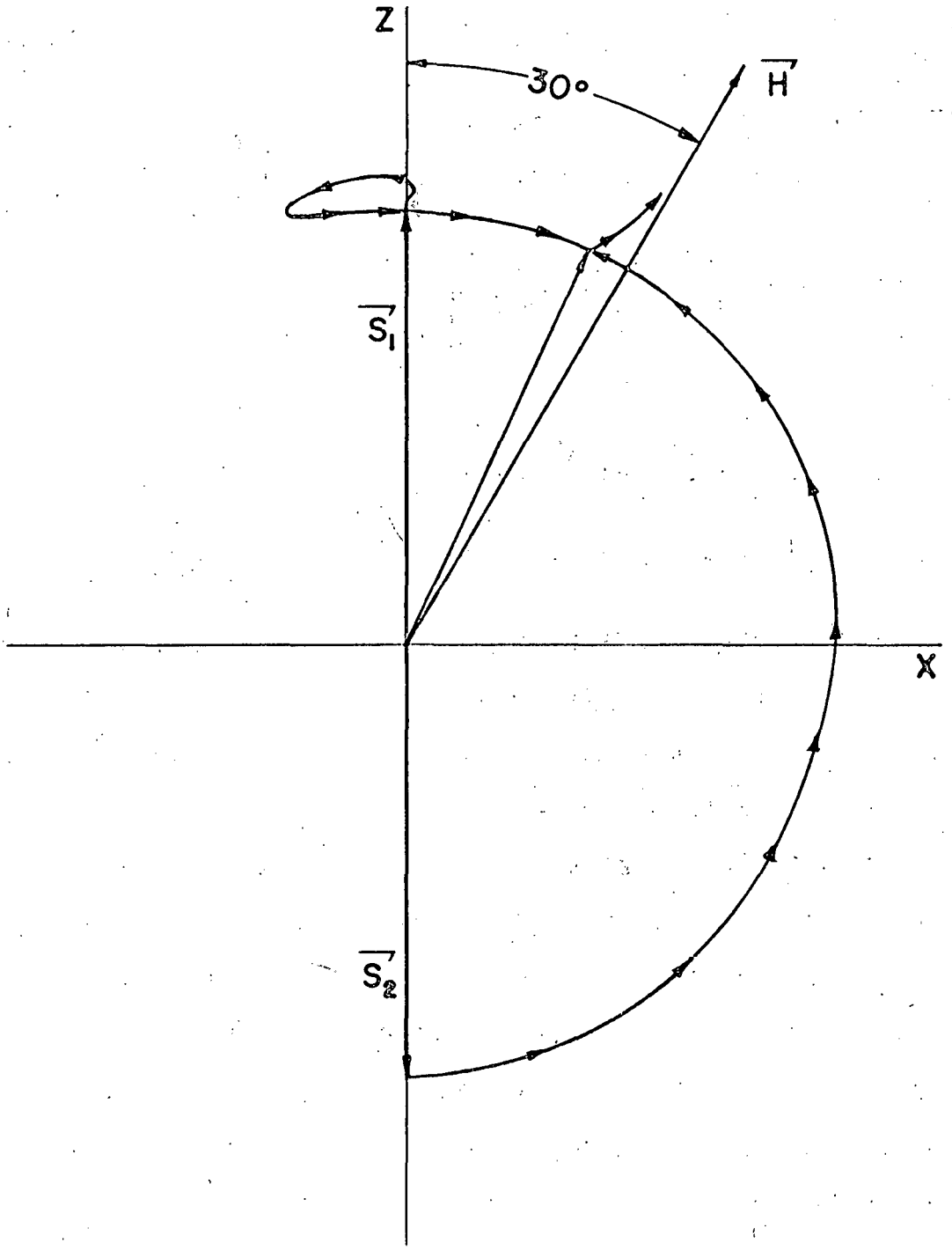
Z
30°
H
S1
X
S2

and λ_2, initially unequal, both approach λ, where

$$(\alpha-\beta) \leq \lambda \leq (\alpha-\beta+K) \quad . \tag{5.77}$$

The limits are independent of the path of approach to the point $\lambda_1=\lambda_2=\lambda$. The resulting expressions are

$$\tan^2\phi = \frac{(\lambda-\alpha+\beta)(\lambda-\alpha-\beta)^2\left[S+(\lambda-\alpha+\beta-K)S'\right]}{(\alpha-\beta+K-\lambda)(\lambda-\alpha-K)^2\left[S+(\lambda-\alpha+\beta)S'\right]} \quad , \tag{5.78}$$

and

$$H_c^2 = (1/K)\left\{(\lambda-\alpha+\beta)(\lambda-\alpha-\beta)^2\left[S^2+(\lambda-\alpha+\beta-K)SS'\right]\right.$$
$$\left. + (\alpha-\beta+K-\lambda)(\lambda-\alpha-\beta-K)^2\left[S^2+(\lambda-\alpha+\beta)SS'\right]\right\} \quad , \tag{5.79}$$

where S is the function of λ given by Eq. (5.4) and S' means the derivative of S with respect to λ. Unfortunately, H_c and tan ϕ are expressed as functions of the parameter λ, so that a little labor is required to get H_c as a function of ϕ.

Consideration of the λ-diagram of Fig. 8, and in particular the free energy vs. external field curves of Fig. 9 for $\phi=0$, makes it seem highly probable that a curve connecting points E and C separates the region AEBCD into a stable region AECD and an unstable region EBC. The contours of constant ϕ for small enough ϕ's, then, would cross into the unstable region and the angular momenta would flop just as they do for $\phi=0$. As ϕ increases away from zero, the loop BCE of Fig. 9 must become rounded and smaller, vanishing for some finite value of ϕ. The computation involved in investigating

the solutions of the equations for small angles is very heavy, and we have not carried through the analysis.

VI. FERROMAGNETIC - ANTIFERROMAGNETIC TRANSITIONS

We examine in this chapter the conditions necessary in the molecular field approximation for magnetic structure transitions to occur in the hexagonal close-packed structure. Let us first consider the conditions which determine the stable state at T=0, when H=0. From Eq. (4.3), all the S_i have the same magnitude

$$S_i = J \quad . \tag{6.1}$$

The equilibrium configuration is that for which the energy E is a minimum, where

$$E = - 2Ng_J\mu_B \sum_{i>j} \gamma_{ij} \vec{S}_i \cdot \vec{S}_j + \sum_i (K/2) S_{iz}^2 \quad . \tag{3.8}$$

When we minimize E subject to conditions (6.1), we find that the stable arrangement is given by Eqs. (4.2) with H=0. The states listed in Tables I and II are solutions of Eqs. (4.2), and furthermore, satisfy conditions (6.1). Therefore, one of these states is the stable configuration for T=0. By combining Eqs. (3.8), (3.12), and (4.1), we write energy E in the form

$$E = - Ng_J\mu_B \sum_i \vec{S}_i \cdot \vec{H}_i = - Ng_J\mu_B \sum_i \lambda_i S_i^2 \quad . \tag{6.2}$$

Since all the λ_i are equal and $S_i=J$, it follows that

$$E = - nNg_J\mu_B J^2 \lambda = - nNg_J\mu_B J^2 T_c/C' \quad , \tag{6.3}$$

where the values of T_c/C' for the various states are given in Tables I and II. Therefore the state with highest critical temperature is the state stable at T=0, if the molecular field coefficients do not change with temperature.

Furthermore, it is easy to show that this same state is stable at high temperatures, if again the molecular field coefficients are constant. To see this, we examine for high temperatures the molecular field equations (3.20) and (4.2) with H=0. The argument of B_J is small for temperatures near the critical temperature, so that we approximate Eq. (3.20) by

$$S_i = C' H_i/T \quad . \tag{6.4}$$

Comparing Eqs. (4.1) and (6.4), we see that for high temperatures

$$\lambda_i = T_c/C' \quad , \tag{6.5}$$

and thus, all the λ's are equal. The solutions of the molecular field equations under the assumption that all the λ_i are equal have already been discussed, and the critical temperatures for the various ordered states are listed in Tables I and II. We see, therefore, that the state associated with the largest λ is the stable state for higher temperatures than any other ordered arrangement.

Since, for molecular field coefficients independent of temperature, the state with the highest critical temperature

is stable both at the absolute zero of temperature and at higher temperatures than any other ordered state, it is reasonable to assume that it is stable throughout the entire temperature range. Therefore, to have magnetic structure transitions in the hcp structure, it appears that the Weiss molecular field coefficients must change with temperature. This conclusion was reached earlier by Smart (6) for the case of cubic structures with $J=\frac{1}{2}$. The question of transitions between different ordered states is discussed also in Appendix B.

The thermal expansion of the structure provides a mechanism for the temperature variation of the molecular field coefficients, which are assumed to depend strongly on the distance between interacting atoms. Following Smart (6), we now assume that the molecular field coefficients are linear functions of temperature, so that λ's for the various ordered states can be written

$$\lambda_m = \lambda_m^\circ(1 + \epsilon_m T) \quad , \tag{6.6}$$

where λ_m° and ϵ_m are different for each ordered state, because each λ_m is a different linear combination of the field coefficients p, q, and r and the anisotropy parameter K. The free energy of Eq. (3.18), for the mth ordered state in zero field, takes the form

$$F_m = nNg_J\mu_B\lambda_m S_m^2 - nkT \ln Z(\mu\lambda_m S_m/kT) \quad , \tag{6.7}$$

where

$$S_m = J\, B_J(\mu\lambda_m S_m/kT) \quad , \tag{6.8}$$

and λ_m is the function of T given by Eq. (6.6). We define a temperature T_T as the temperature at which the transition from one ordered state to another occurs in zero magnetic field.

By examining Eq. (6.7), we can find the conditions which allow a transition between the mth and nth ordered states. If state m is stable above T_T, and state n stable below, then

$$\lambda_m(T) > \lambda_n(T) \text{ for } T>T_T \quad ,$$

$$\lambda_m(T) = \lambda_n(T) \text{ for } T=T_T \quad ,$$

$$\lambda_m(T) < \lambda_n(T) \text{ for } T<T_T \quad . \tag{6.9}$$

We are interested particularly in examining the conditions under which a transition can occur between ferromagnetic state F and one of the antiferromagnetic states. The anisotropy coefficient K may also vary with temperature, but for lack of information, we choose to neglect this variation, so that the coefficient K plays no role in the transition. We look for conditions on p, q, and r which allow transitions between F and one of the antiferromagnetic states A_i to occur. The criteria for a transition between states F and A_i is that they both be stable relative to the disordered state ($\lambda_F>0$, $\lambda_{Ai}>0$), that λ_F and λ_{Ai} be greater than λ's for the

other ordered states, and finally that λ_F and λ_{Ai} are nearly equal. When these criteria are applied to the states in Table I, it is found that F-A_i transitions could occur under the conditions given in Table III.

Table III. Possible F-A_i transitions in the hcp structure, and the conditions under which they could occur. (It is assumed that the anisotropy coefficient K does not change sign.)

Transition	Conditions for Occurrence
F-A	$p>\|q\|$; $3q+r \simeq 0$
F-B	$r>0$; $-2r<(p-q)<2r/3$; $p+q \simeq 0$
F-C	$q>\|p\|$; $-3q<r<q$; $2p+q+r \simeq 0$

We now assume for definiteness that the ferromagnetic-antiferromagnetic transition occurs between states F_z and A_z, as discussed in Appendix B, and that the structure is subdivided into two sublattices. There are four constants λ_{Az}°, λ_{Fz}°, ϵ_{Az}, and ϵ_{Fz} to determine. If we assume that state A_z is stable above the transition temperature T_T, then its critical temperature is the Néel point which is observed experimentally. The critical temperature T_{Az} of state A_z is the highest temperature for which a non-zero solution of Eq. (6.8) can be found, with $\lambda_i=\lambda_{Az}$. By taking the derivative of both sides of Eq. (6.8) with respect to S_m, setting $S_m=0$, and taking λ_{Az} as a linear function of temperature of the

form (6.6), we find that T_{Az} is given by

$$T_{Az} = C'\lambda_{Az}\circ(1 - C'\lambda_{Az}\circ\epsilon_{Az})^{-1} \quad . \tag{6.10}$$

We have given in Eq. (5.35) the formula for the paramagnetic susceptibility of the system, which can be written with the aid of the relation $(T_{Fz} - T_{Fx} = T_K)$

$$\chi = \frac{C\ 3(T-T_{Fz})+2T_K}{3(T-T_{Fz})(T-T_{Fz}-T_K)} \quad . \tag{6.11}$$

Therefore, T_{Fz} can be obtained from the experimental data, and we have in analogy with Eq. (6.10) the relation

$$T_{Fz} = C'\lambda_{Fz}\circ(1 - C'\lambda_{Fz}\circ\epsilon_{Fz})^{-1} \quad . \tag{6.12}$$

Since at temperature T_T

$$\lambda_{Fz}(T_T) = \lambda_{Az}(T_T) \quad , \tag{6.13}$$

this provides a third relation between the constants:

$$\lambda_{Fz}\circ(1+\epsilon_{Fz}T_T) = \lambda_{Az}\circ(1+\epsilon_{Az}T_T) \quad . \tag{6.14}$$

There is, therefore, one molecular field parameter to adjust, which can be chosen so that the temperature coefficients ϵ_{Az} and ϵ_{Fz} are of reasonable magnitude. Néel (33) has discussed the expected order of magnitude for the temperature coefficients of the molecular field parameters and has estimated a value of $10^{-4}/°K$ for the order of magnitude.

If we choose for our arbitrary constant the value of

$\lambda_{Fz}(T_T)$ and $\lambda_{Az}(T_T)$, we can express all the parameters as functions of $\lambda_{Fz}(T_T)$, or equivalently, of the function

$$Q = 3J\left[x(J+1)\right]^{-1} B_J(x) \quad , \tag{6.15}$$

where

$$x = \mu\lambda_{Fz}(T_T)S_{Fz}/kT \quad . \tag{6.16}$$

We find that

$$\epsilon_{Az} = (Q/T_T - 1/T_{Az}) \quad , \tag{6.17}$$

$$\epsilon_{Fz} = (Q/T_T - 1/T_{Fz}) \quad . \tag{6.18}$$

When ϵ_{Az} and ϵ_{Fz} are known, $\lambda_{Az}{}^{\circ}$ and $\lambda_{Fz}{}^{\circ}$ can be obtained from Eqs. (6.10) and (6.12). Fortunately, when we calculate ϵ_{Az} and ϵ_{Fz} as functions of Q, we find that they are of the order of magnitude of $10^{-4}/^{\circ}K$ for only a relatively small range of values of Q.

The data (2, 3) show that for dysprosium

$$T_{Fz} = 157^{\circ}K \quad ,$$

$$T_{Az} = 176^{\circ}K \quad ,$$

$$T_T = 85^{\circ}K \quad . \tag{6.19}$$

The values of the parameters we have chosen for the subsequent exploratory calculations are given in Table IV, where we have included a value for the parameter K which

Table IV. Values of the parameters used in the investigation of ferromagnetic-antiferromagnetic transitions in the molecular field approximation.

Parameter	Value
$\lambda_{Az}{}^{\circ}$	8.744×10^{4} oersteds
$\lambda_{Fz}{}^{\circ}$	9.858×10^{4} oersteds
K	1.576×10^{3} oersteds
ϵ_{Az}	$7.497 \times 10^{-4}/^{\circ}K$
ϵ_{Fz}	$-6.649 \times 10^{-4}/^{\circ}K$

allows spin flop to occur for orders of magnitude of the external magnetic field which agree with the experimental results for dysprosium. These are also the coefficients used in all the quantitative calculations of Chapter V and represented in Figs. 7 through 11.

In all the calculations of Chapters V and VII, we have taken $J=15/2$ and $g_{15/2}=4/3$. These values, which are appropriate for the 4f shell of dysprosium (23, p. 243), lead to an effective magnetic moment per atom of $10.65\mu_B$, for temperatures above the Néel temperature. The experimentally measured effective magnetic moment per atom is $10.64\mu_B$, for temperatures from 177 to 730°K(1).

VII. COMPARISON OF THEORY AND EXPERIMENT

A. The Susceptibility for Weak Applied Fields

In the previous chapters, we have derived the solutions of the molecular field equations for arbitrary magnitudes and directions of the applied magnetic field. We consider in this chapter the predictions of our model concerning the magnetic properties of dysprosium metal. For all calculations, the values used for the molecular field coefficients and the anisotropy parameter K are given in Table IV.

In order to have a change between ordered phases, it is necessary to assume that λ_{Az} and λ_{Fz} vary with temperature. The calculations of this section are carried out under the assumption that λ_{Az} and λ_{Fz} are linear functions of temperature of form (6.6). At the temperature T_T of the P-A transition, we recall from Eq. (6.9) that $\lambda_{Az}(T_T) = \lambda_{Fz}(T_T)$, which implies that $T_{Az}(T_T) = T_{Fz}(T_T)$. The theoretical susceptibility χ_{11}, for fields parallel to the preferred axis, is given by Eq. (5.57), and behaves like that of a normal antiferromagnetic, since it decreases monotonically with decreasing temperature. However, $\chi_{\perp}$, the susceptibility for fields perpendicular to the preferred axis, is given by Eq. (5.75). It steadily increases to a very large value as the temperature decreases from 176°K, the Néel temperature for the antiferromagnetic state, to 85°K, the transition temperature T_T. This behavior is to be contrasted with

that of a normal antiferromagnetic, where $\chi_\perp$ stays nearly constant. The susceptibilities $\chi_\parallel$ and $\chi_\perp$ are shown as functions of temperature in Fig. 12. The experimental susceptibility obtained from the data of Elliott, Legvold and Spedding (3) is shown in Fig. 13. When K>0, so that the axis of alignment of the angular momenta is the z axis, it follows that

$$\chi_{av} = (2\chi_\perp + \chi_\parallel)/3 \quad , \qquad (7.1)$$

where χ_{av} is the theoretical susceptibility for a polycrystalline sample with crystallites randomly oriented and is plotted in Fig. 12 as a function of T. The susceptibility χ_{av} drops and then rises as the temperature decreases from the Néel temperature, thus accounting qualitatively for similar behavior in the experimental susceptibility of Fig. 13. If this explanation is correct, the susceptibility for a single crystal in any one direction would not show this behavior. On the other hand, the single crystal susceptibility should be strongly anisotropic at temperatures well below the Néel point, an effect which would provide an interesting test of the predictions of our calculations.

If we take K<0, the direction of alignment of the angular momenta in zero field is perpendicular to the z axis. With the simple form we have assumed for the anisotropy, there is then no preferred direction in the x-y plane and the angular momenta would align perpendicular to the applied field for fields along the x and y, as well as the z axes.

Fig. 12. The theoretical susceptibilities $\chi_{\parallel}$, $\chi_{\perp}$, and χ_{av} as functions of temperature, when the molecular field coefficients are taken as linear functions of the temperature of form (6.6). Susceptibility $\chi_{\parallel}$ is given by Eq. (5.57), $\chi_{\perp}$ by Eq. (5.74), and χ_{av} by Eq. (7.1).

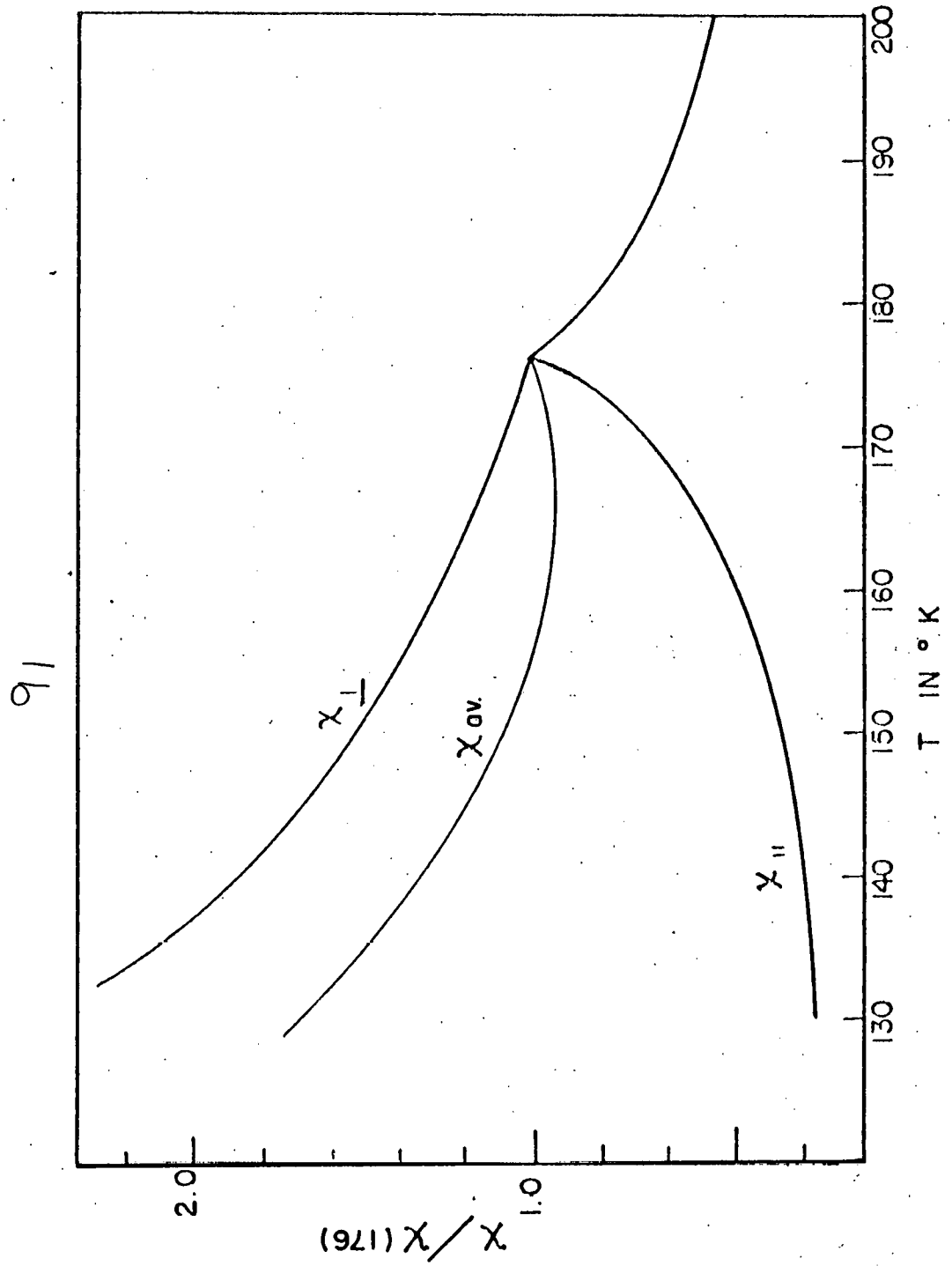
91
$\chi_{\perp}$
$\chi_{av.}$
$\chi_{\parallel}$
2.0
1.0
$\chi / \chi(176)$
200
190
180
170
160
150
140
130
T IN °K

Fig. 13. The initial susceptibility of dysprosium, from the data of Elliott, Legvold, and Spedding (3).

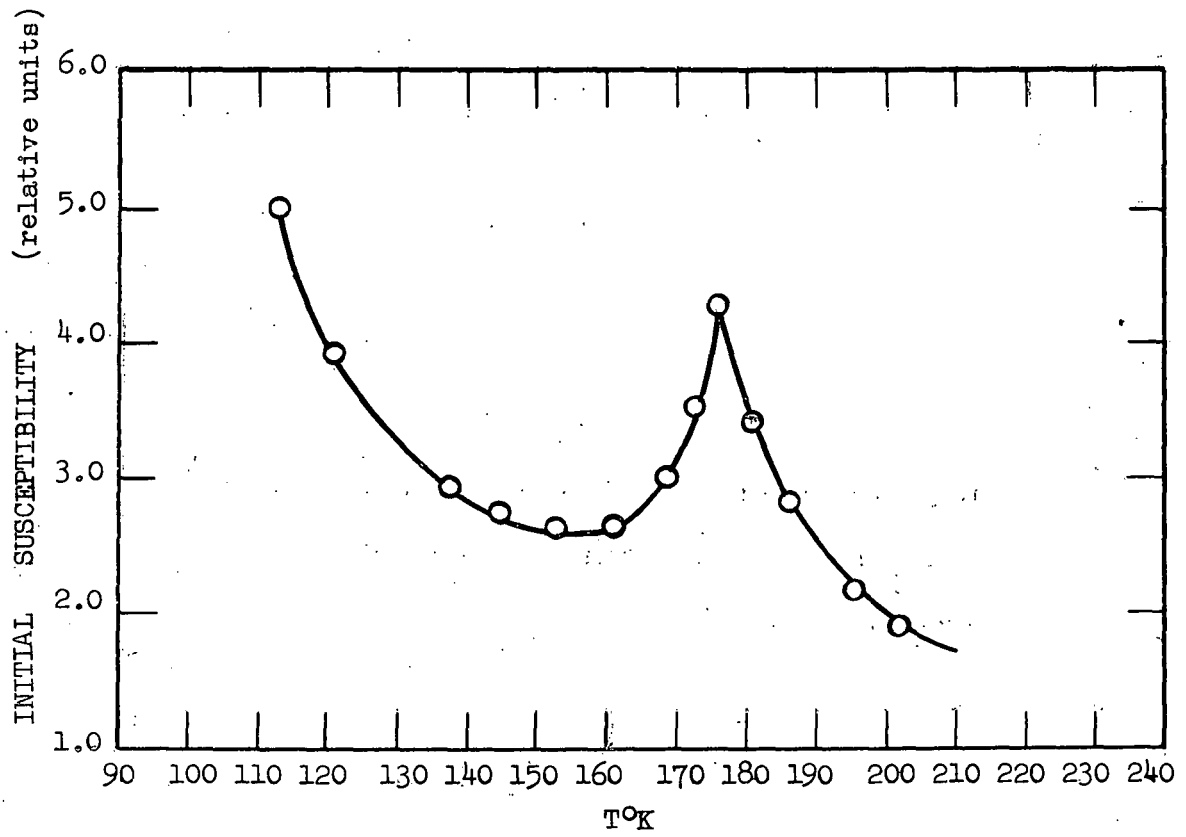
INITIAL SUSCEPTIBILITY (relative units)
6.0
5.0
4.0
3.0
2.0
1.0
90 100 110 120 130 140 150 160 170 180 190 200 210 220 230 240
T°K

Fig. 14. The heat capacity of dysprosium, from the data of Griffel, Skochdopole, and Spedding (4).

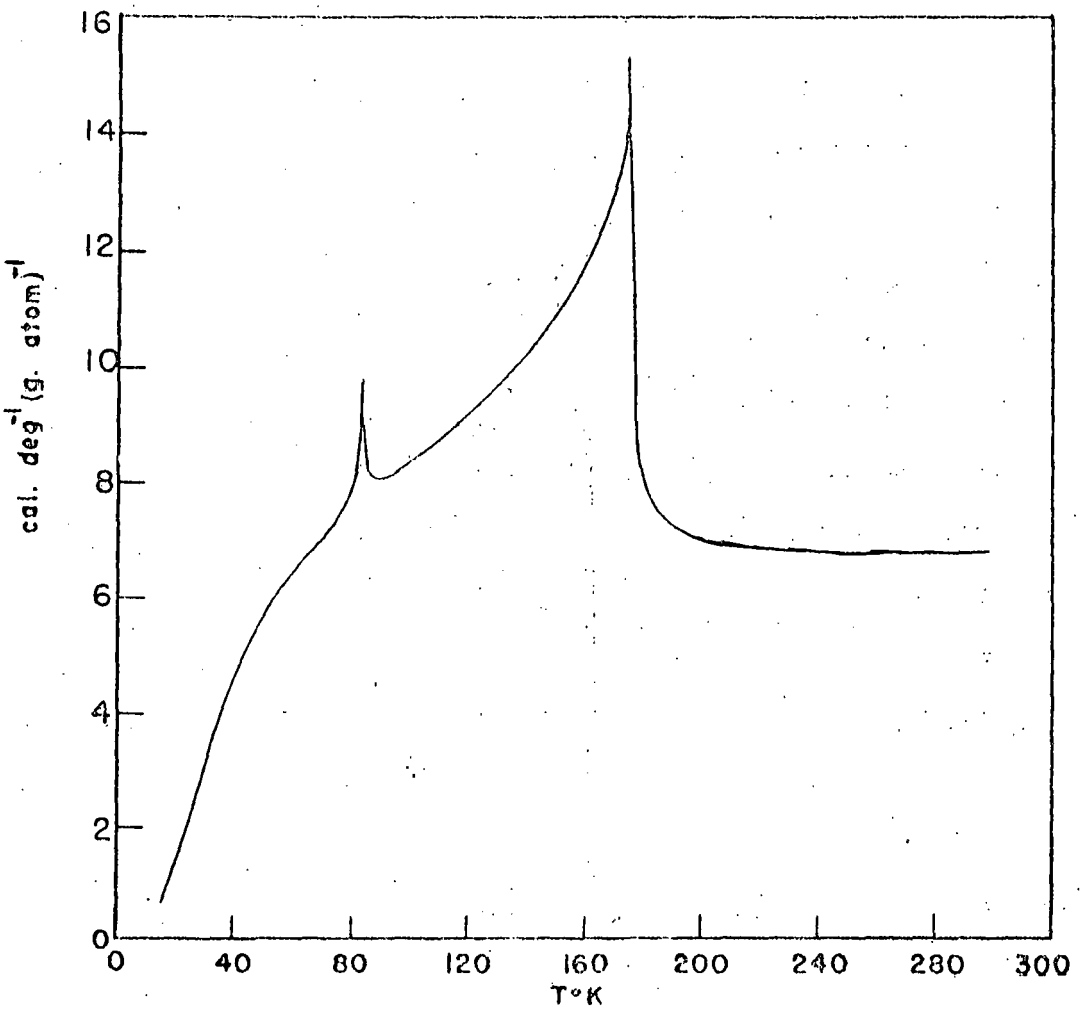
16
14
12
10
8
6
4
2
0
cal. deg^{-1}(g. atom)$^{-1}$
0
40
80
120
160
200
240
280
300
T°K

The susceptibilities along all three axes would then increase steadily as the temperature decreases. The polycrystalline susceptibility χ would have no minimum in this case. If however, some form of anisotropy were present, caused by strains in the crystallites or by small anisotropic interatomic interactions which we have neglected, the experimental χ would again be given by Eq. (7.1).

The long range of temperature over which the experimental susceptibility rises is accounted for in our model by the behavior of the susceptibility $\chi_\perp$, which starts to rise at the Néel temperature and increases to a very large value at the transition temperature T_T. At first it was thought that the rise in susceptibility could be explained by the presence of short range ferromagnetic order in the antiferromagnetic state. This explanation seems unlikely however, since the peak in the heat capacity at 85°K, shown in Fig. 14, is very sharp and does not seem to have the large tail characteristic of the presence of short range order.

B. The Behavior of the System in Strong Magnetic Fields

In our model, the molecular field coefficients have been chosen so that state A_z is stable for zero field and temperatures between 85 and 176°K. State A_x is unstable relative to A_z because its angular momenta are aligned perpendicular to the preferred axis. Ferromagnetic state F is unstable above 85°K because, with its angular momentum

arrangement, the free energy of exchange is higher than for state A_z. With molecular field coefficients that vary with temperature, the relative importance of the exchange and anisotropy energies changes. This effect shows up clearly if we examine the behavior of the system as a function of F for fields directed along the z axis. We have already described the phenomenon of spin flop in Chapter V. Equation (5.69) gives approximately H_f, the threshold field at which spin flop occurs, as a function of temperature. Figure 15 shows H_f as a function of T (the curve designated by the symbol X), as calculated using approximation (5.69) for the whole temperature range in question.

We wish also to analyze as a function of temperature the magnetic field strengths for which states A_x and F become identical. The properties of A_x are described in Chapter V, where it is shown that A_x can exist only for fields less than a critical field H_c given by

$$H_c = -(2\beta+K)S_{Ax} \quad , \qquad (7.2)$$

which is obtained by setting $H_{cx} = 0$ in Eq. (5.42), and where S_{Ax} is obtained from Eq. (5.4) with $\lambda_1 = \alpha-\beta$. For fields above H_c, only state F can exist. The field H_c as a function of T is shown in Fig. 15 by the curve marked with the symbol $\triangle$.

The relative stability of states A_z and F can be examined for $\phi = 0$ by using approximation (5.61) for the

9f

Fig. 15. The H-T diagram showing the stable state at temperature T and its dependence upon the magnitude of the applied field H, when H is directed along the z axis. The letters F, A_x, and A_z give the type of order which is stable in each of the regions bounded by the solid curves. The solid curves represent values of H and T for which transitions occur between ordered states.

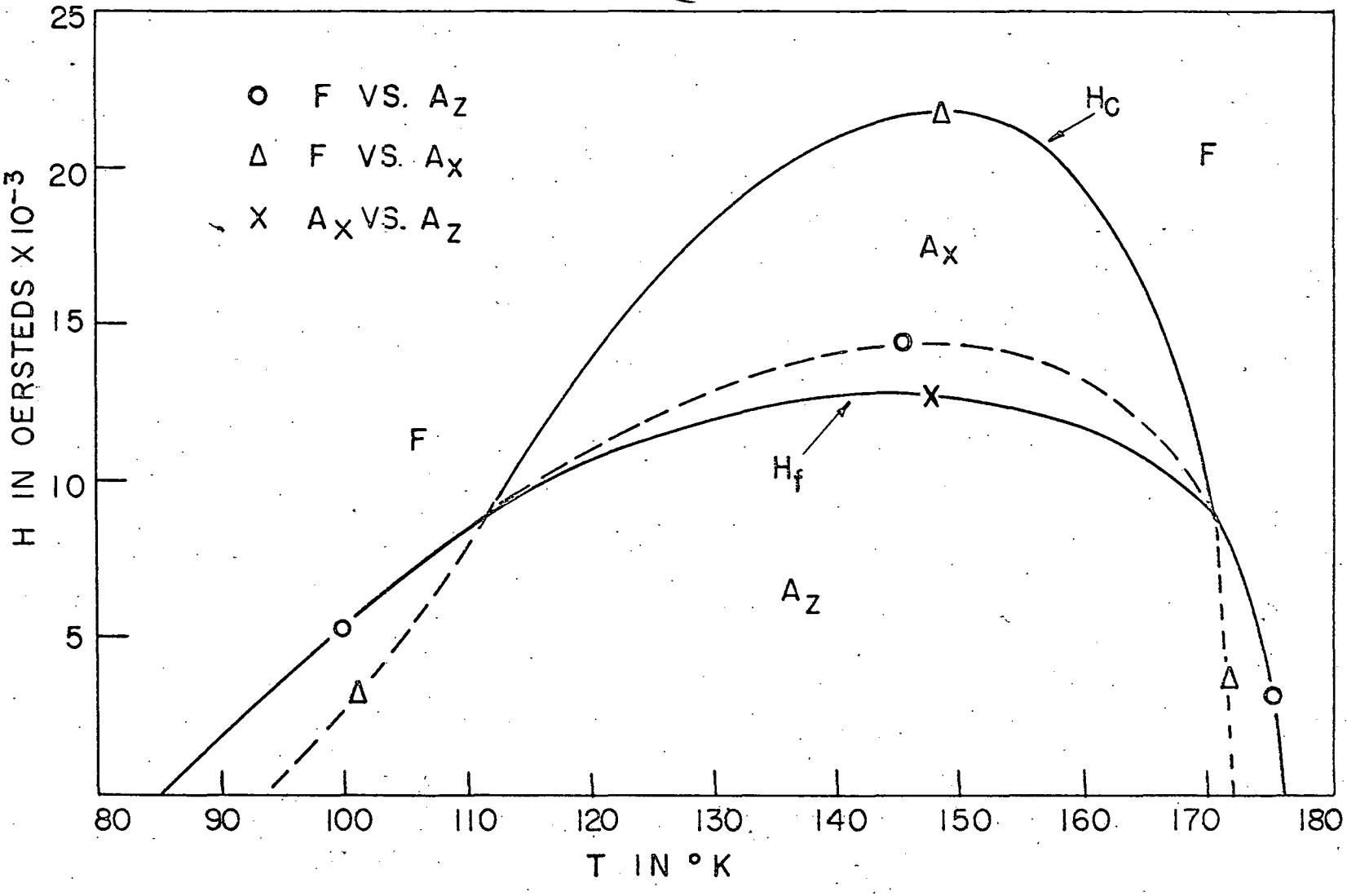
O F VS. A_Z
Δ F VS. A_X
X A_X VS. A_Z
H_C
F
A_X
F
H_f
A_Z
H IN OERSTEDS X 10^{-3}
25
20
15
10
5
80
90
100
110
120
130
140
150
160
170
180
T IN °K

free energy of A_z and calculating the free energy of F exactly from Eq. (3.21) with $\lambda_1=\lambda_2=\lambda$. The result of this calculation is given in Fig. 15, where the curve marked by the symbol O represents the critical values of the field for which the free energies of states A_z and F are equal.

For temperatures close to 85°K and 176°K, the field reaches the value H_c before state A_x becomes more stable than A_z. Therefore, for these ranges of temperature, the competition is between states A_z and F. The ranges of temperature in question are from 85 to 112°K and from 171 to 176°K, approximately, as indicated in Fig. 15. The solid portions of the curve marked with the symbol O represent the boundary between states A_z and F in the H-T plane, for $\phi=0$. A discontinuity in magnetization occurs when the field exceeds the value on this curve for temperatures between 85 and 112°K, but not for the range from 171 to 176°K. Although the term spin flop is generally used to the discontinuous change of spin direction which occurs when the system changes from state A_z to A_x, we extend its meaning to include also the discontinuous change associated with the switch from state A_z to F.

In Fig. 15, the curves drawn with solid lines represent as functions of temperature the fields for which changes in ordering occur. We notice that in the intermediate temperature range two changes occur, the change A_z to A_x followed by A_x to F. The former change is accompanied by the

discontinuity in magnetization shown in Fig. 10, which gives magnetization curves for T=143.6°K.[1] The magnetization is continuous for the latter change, but the susceptibility is discontinuous.

The discussion of this section (and Fig. 15) has all been for the external magnetic fields along the z axis (ϕ=0). We call attention also to the magnetization curves for ϕ=30° and ϕ=90° in Fig. 10. Measurement of the magnetization as a function of the magnitude and direction of the applied magnetic field and as a function of temperature for a single crystal of dysprosium would provide an interesting test of the predictions of our theory. The magnetization curves for different temperatures in the range for which spin flop is predicted would all look qualitatively similar to the curves in Fig. 10.

Some interesting predictions can be made from the H-T diagram of Fig. 15 for $\vec{H}$ directed along the z axis. For example, it is apparent that the temperature at which the F-A transition occurs is a strong function of the magnitude of the applied field, an effect which could be looked for in specific heat measurements. The field variation of the temperature T_T of the F-A transition would yield data which

[1]Rather high precision was required in carrying out the numerical calculations. The particular temperature 143.6°K is not significant. It lies in the middle of the range of temperature for which spin flop occurs, and it happens to make the solution of certain transcendental equations easier.

Fig. 16. Representative magnetization curves for dysprosium, from the data of Elliott, Legvold, and Spedding (3).

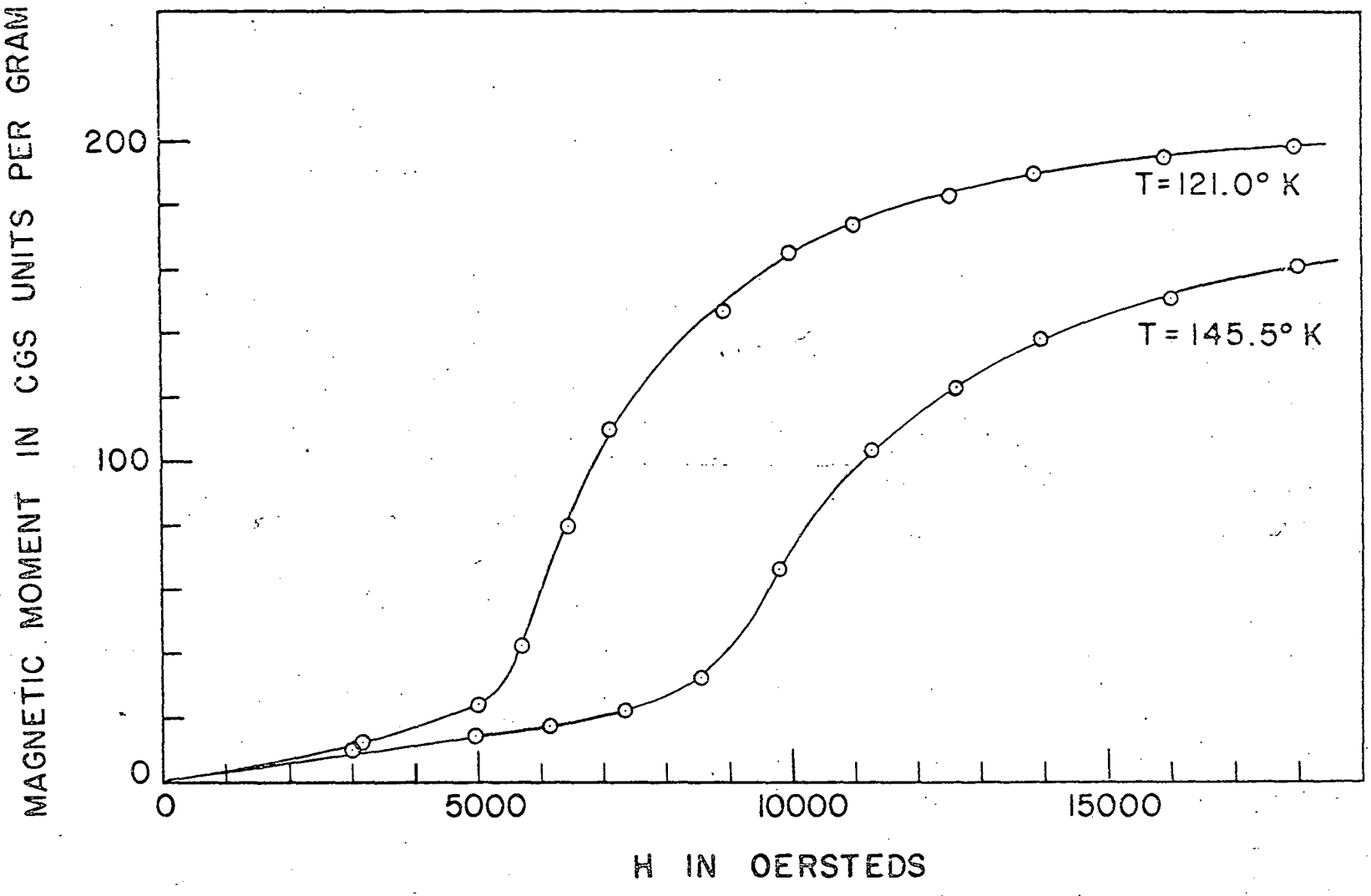
MAGNETIC MOMENT IN CGS UNITS PER GRAM
200
100
0
0
5000
10000
15000
H IN OERSTEDS
T=121.0° K
T=145.5° K

would help determine completely the four parameters we have introduced for the temperature variation of the molecular field coefficients. Another effect shown in Fig. 15 is that for small magnetic fields the transition is from F to A_z, while for large fields it is F to A_x. Neutron diffraction measurements could detect this effect, since they would enable the direction of alignment of the spins to be determined as well as the presence of superlattice lines for the state A_x. It is also apparent that for large fields the F-A transition does not occur at all.

We now compare the predictions of our model on magnetization curves with the experimental data for polycrystalline dysprosium. To make a quantitative prediction, we would need to know the magnetization for a single crystal as a function of the magnitude and direction of the applied field, so that we could calculate the magnetization for a sample in which the crystallites are randomly oriented. We can see at least qualitatively, however, what the answer will be by examining the theoretical magnetization curves of Fig. 10 for ϕ=0, 30, and 90° and T=143.6°K. A properly weighted average of the three curves would look rather similar to the magnetization curves in Fig. 16, which are taken from the data of Elliott, Legvold, and Spedding (3).

From the standpoint of our model, we interpret the experimental curves of Fig. 16 as follows. For the low field portions of the curves, the effect of the magnetic field is

small compared to the anisotropy, so that the angular momenta remain more or less aligned along the z axis, and the net magnetization of the sample is small. The magnetization curves rise rapidly when the magnetic field overcomes the anisotropy, corresponding to the large susceptibility perpendicular to the direction of preferred alignment. The magnetization curves level off for large fields, when the antiferromagnetic state has become identical with state F (paramagnetic saturation). A weighted average of the magnetization curves of Fig. 10 would seem to give a predicted magnetization for a polycrystalline sample which does not rise as steeply as the experimental magnetization. This comes about because the 90° curve is weighted more heavily than the 0° curve in taking the average.

We also see now the essential role that the anisotropy plays, since if it were absent, the polycrystalline magnetization curves would look like the curve for $\phi=90°$ in Fig. 10. The field H_f for which spin flop occurs is determined by the magnitude of the anisotropy, as follows from Eq. (5.69). We can deduce the size of the anisotropy from the experimental data if we make the reasonable assumption that H_f is the field for which the experimental magnetization curves begin to depart rapidly from their low field linearity. We compare in Fig. 17 the experimental H_f determined this way and the theoretical H_f calculated from Eq. (5.69). The curves do not agree quantitatively, which is not surprising

Fig. 17. Field H_f as a function of T from theory and experiment.

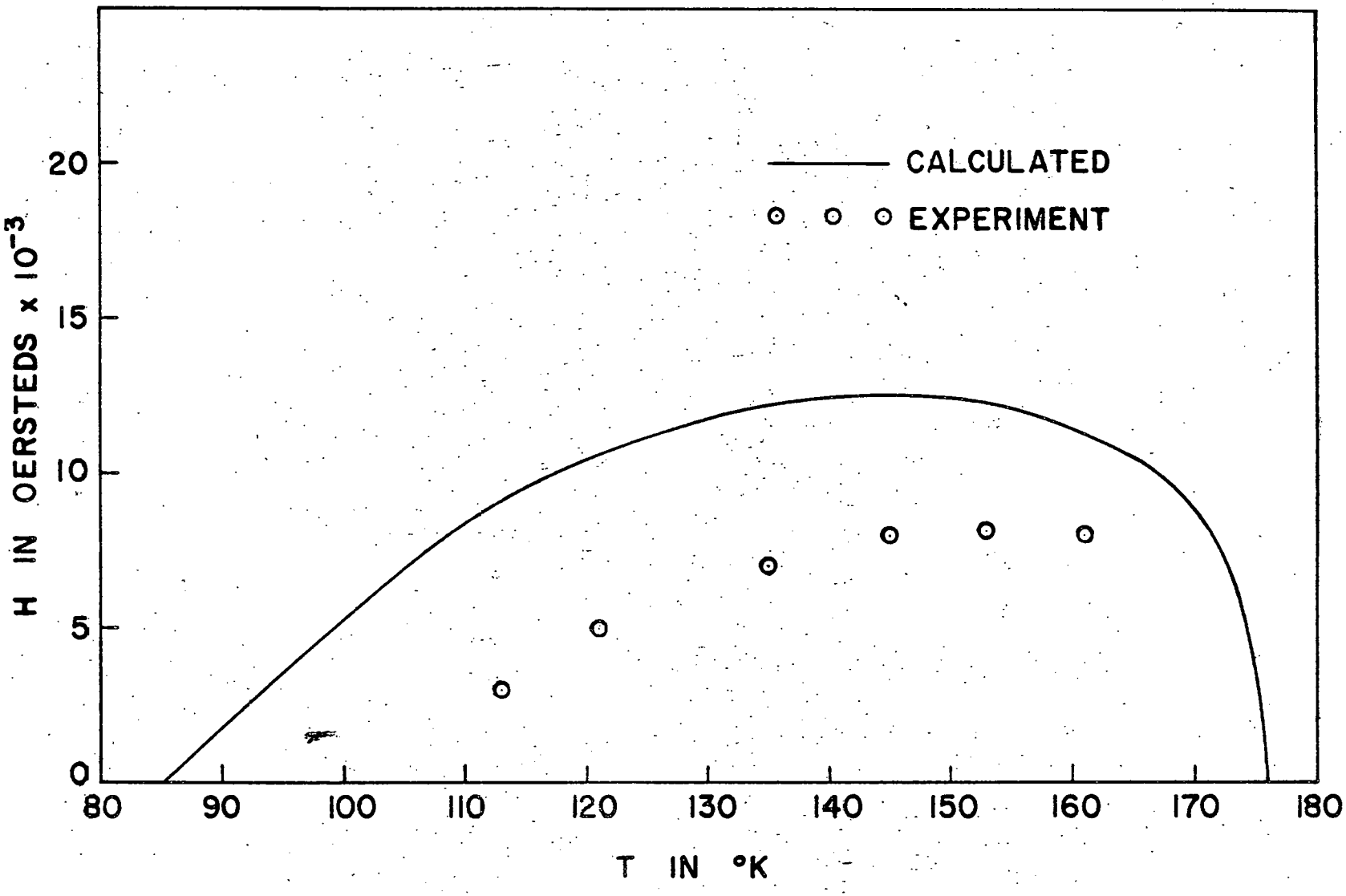
CALCULATED
EXPERIMENT
H IN OERSTEDS x 10^{-3}
T IN °K
0
5
10
15
20
80
90
100
110
120
130
140
150
160
170
180

since the value of K used was merely a careful guess. However, on the basis of this comparison we could improve the value of K for future calculations by taking a lower value. The theoretical and experimental curves for H_f agree qualitatively in shape at least, since they both flatten out for higher temperatures.

The field H_c, which represents the critical field at which the ferromagnetic and antiferromagnetic states have the same free energy for ϕ not too close to zero, is given by Eqs. (5.78) and (5.79). It appears that H_c is a rather complicated function of ϕ and T. Although we have not carried out the analysis, we expect that for a polycrystalline sample in a magnetic field the heat capacity anomaly associated with the F-A transition will become smeared out, because the transition temperature of each crystallite will depend upon its orientation relative to the field. For magnetic fields parallel to the z axis, the displacement of transition temperature T_T of the F-A transition is shown in Fig. 15 by the lower branch of the solid curve marked by the symbol 0, which starts at the point T=85°K, H=0. For fields perpendicular to the z axis ($\lambda=\alpha-\beta+K$), the values of H and T for which the F-A transition occurs are obtained from Eqs. (5.78) and (5.79) and lie on the curve

$$H_c = (-2\beta+K)S \quad , \tag{7.3}$$

with

$$S = J B_J\left[\mu(\alpha-\beta+K)S/kT\right] \quad . \qquad (7.4)$$

It is a consequence of Eq. (7.3) that the displacement of T_T is less for H perpendicular to the z axis than for H parallel. The field required to suppress the F-A transition altogether in a polycrystalline sample is given by the maximum value of H_c as a function of temperature. The Néel temperature is also changed by the presence of a magnetic field, although less strongly than T_T. This effect is shown in Fig. 15 by the upper branch of the solid curve marked by the symbol O, which passes through the point T=1.76 °K, H=0.

C. Thermodynamic Nature of the Magnetic Transitions

The high temperature antiferromagnetic to paramagnetic transition is an ordinary second order transition. If we take seriously the expression for the free energy given by Eq. (3.21), then we predict that the F-A transition is of first order. This result agrees with that of Smart (6) for the special case $J=\frac{1}{2}$. However, it must be emphasized that the temperature dependence of the molecular field coefficients - an essential feature of the molecular field theory of the F-A transition - was not introduced in a consistent way, but was thrown in after the free energy expression was derived. A proper derivation would have to proceed by considering the molecular field coefficients as explicit functions of the lattice parameters, and then calculating the Gibbs function for a given applied pressure, rather than working from the Helmholtz free energy at constant volume - as has been done in our work.

The expected change in entropy at the F-A transition and the associated latent heat of transformation will now be computed from our model. The entropy S is obtained from the free energy F by the relation

$$S = -\partial F/\partial T \quad . \tag{7.5}$$

For the ith ordered state in zero field, F can be written according to (3.21) and (3.22) as

$$F_i = nkT\left[(Nx_iS_i/J) - \ln Z_i\right] \quad , \tag{7.6}$$

with

$$x_i = \mu\lambda_i S_i/kT \quad , \tag{7.7}$$

$$S_i = J\, B_J(x_i) \quad , \tag{7.8}$$

$$\lambda_i = \lambda_i{}^{\circ}(1+ \epsilon_i T) \quad , \tag{7.9}$$

$$Z_i = \left[\sinh\frac{(2J+1)x_i}{2J} \Big/ \sinh\frac{x_i}{2J}\right]^{2N} \quad . \tag{7.10}$$

From Eqs. (7.7) and (7.9), we have

$$T = \mu\lambda_i{}^{\circ}S_i/(kx_i - \mu\lambda_i{}^{\circ}\epsilon_i S_i) \quad . \tag{7.11}$$

A convenient technique for carrying out the derivative with respect to T of Eq. (7.6) is to consider F_i and T as functions of the parameter x_i, so that

$$S = -\,(dF/dx_i)/(dT/dx_i) \quad . \tag{7.12}$$

Without giving the details, we assert that the entropy for the ith state, denoted by the symbol S(i), is given by

$$S(i) = nk\left[\ln Z_i - (2Nx_iS_i/J) + (N\mu\lambda_i{}^{\circ}\epsilon_i S_i{}^2/Jk)\right] \quad . \tag{7.13}$$

The change in entropy ΔS associated with the F-A transition is

$$\Delta S = nNg_J\mu_B(\lambda_A \circ \epsilon_A - \lambda_F \circ \epsilon_F)\, S^2(T_T) \quad , \qquad (7.14)$$

which for the constants we have chosen for our exploratory calculation has the value per gram atomic weight of

$$\Delta S = 0.21\ R \quad . \qquad (7.15)$$

This is a rather large fraction of the total magnetic entropy, and would lead to a measurable latent heat at the F-A transition. The data of Griffel, Skochdopole, and Spedding (4) do not establish conclusively whether the F-A transition is of first order with a small latent heat, or of second order. The entropy S(i) of Eq. (7.13) has a constant value of R ln 16 or 5.506 cal deg^{-1} (g atom)$^{-1}$ for temperatures greater than the Néel temperature. The experimental value for the magnetic contribution to the entropy of dysprosium at 300°K has been determined by Griffel, Skochdopole, and Spedding (4) to be 5.616 cal deg^{-1} (g atom)$^{-1}$.

We should emphasize, however, that ΔS calculated above depends solely upon the parameters we have introduced arbitrarily for the temperature variation of the molecular field coefficients, and not upon any fundamental property of the system. Therefore, we do not believe that our calculation makes a valid prediction either for the order of the F-A transition or for the magnitude of the latent heat. The same criticism applies to the derivation of Smart (6) for the order of the F-A transition and the change of

entropy associated with it.

The heat capacity C(i) for the ith ordered state in zero applied magnetic field can be calculated from Eq. (7.13) by applying the relation

$$C(i) = T\, dS(i)/dT, \tag{7.16}$$

which yields

$$C(i) = (2nNk/J)\, x_i^2 s_i s_i' (s_i - x_i s_i')^{-1}. \tag{7.17}$$

There is the usual discontinuity in C(i) at the Néel temperature, which is given by

$$\Delta C(i) = 80nNkJ^2(J+1)^2\left[(2J+1)^4 - 1\right]^{-1}. \tag{7.18}$$

For dysprosium, where $J = 15/2$, Eq. (7.18) gives for $\Delta C(i)$ a value of 2.48 R or 4.90 cal deg^{-1}(g atom)$^{-1}$. This value is to be compared to a value of about 8.00 cal deg^{-1}(g atom)$^{-1}$ which can be estimated from the heat capacity curve given in Fig. 14. The two values agree in order of magnitude, which is the agreement expected in the molecular field approximation, because of its failure to take into account properly the short range order effects which predominate at the Néel temperature.

The heat capacity of dysprosium shown in Fig. 14 has a very large peak at a temperature of 174°K, which lends strong support to the interpretation that an important magnetic ordering takes place near this temperature. Since

the metal does not have a permanent magnetization for temperatures above 85°K, this has been the principal basis for concluding that dysprosium is antiferromagnetic between 85°K and the Néel temperature of 174°K.

VIII. SUMMARY

The molecular field approximation has been applied to the study of ferromagnetic-antiferromagnetic phase transitions in dysprosium metal. Both ferromagnetic and antiferromagnetic interatomic interactions are assumed to exist in the structure, and they are taken to vary slightly with temperature. In addition, an anisotropy energy has been introduced which arises from the effect of crystal fields.

The molecular field equations for zero applied magnetic field have been investigated and several ordered arrangements for the structure have been derived. Solutions of the equations have been found for arbitrary magnitude and direction of the applied magnetic field.

From our model, we make the following predictions concerning the magnetic behavior of single crystals of dysprosium.

1. For temperatures in the antiferromagnetic range, we predict a large anisotropy in the single crystal susceptibility. The susceptibility $\chi_{\parallel}$, for weak fields parallel to the preferred axis, behaves like that of a normal antiferromagnetic, decreasing steadily with decreasing temperature. The susceptibility $\chi_{\perp}$, for weak fields perpendicular to the preferred axis, increases strongly and monotonically as the temperature decreases.

2. For temperatures in the antiferromagnetic range and for fields making small angles with the preferred axis of alignment of the angular momenta, the phenomenon of spin flop occurs. The angular momenta undergo a sudden change in their directions of alignment, and the corresponding magnetization curves are discontinuous.
3. The transition temperature T_T of the F-A transition for magnetic fields parallel to the preferred axis is a strong function of the applied field, increasing with increasing field. For small constant magnetic fields, the transition is between state F and A_z. For larger fields it is F - A_x. Finally, when the magnetic field exceeds a certain critical value, the F-A transition does not occur at all and the system remains in state F.

The following results are obtained for polycrystalline dysprosium.

1. The behavior of the experimentally measured susceptibility, which increases rapidly over a wide range of temperatures in the antiferromagnetic range as the temperature decreases, is accounted for by the rapid rise in the susceptibility $\chi_\perp$.
2. The sharp peak in the heat capacity at the temperature of the F-A transition should become smeared out in the presence of large magnetic fields. This should happen because the transition temperature for a single crystal depends upon the orientation of the magnetic field relative to the crystal.

IX. LITERATURE CITED

1. Trombe, F. Ferromagnétisme et paramagnétisme du dysprosium métallique. Compt. rend. 221, 19 (1945).

2. Trombe, F. Le dysprosium métallique et ses propriétés magnétiques. J. recherches centre natl. recherche sci., Lab. Bellevue (Paris), no. 23 (1953).

3. Elliott, J. F., Legvold, S., and Spedding, F. H. Some magnetic properties of Dy metal. Phys. Rev. 94, 1143 (1954).

4. Griffel, M., Skochdopole, R. E., and Spedding, F. H. The heat capacity of dysprosium from 15 to 300°K. J. Chem. Phys. (in press).

5. Banister, J. R., Legvold, S., and Spedding, F. H. Structure of Gd, Er, and Dy at low temperatures. Phys. Rev. 94, 1140 (1954).

6. Smart, J. S. Magnetic Structure Transitions. Phys. Rev. 90, 55 (1953).

7. Weiss, P. L'hypothèse du champ molécular et la propriété ferromagnétique. J. de Physique 6, 661 (1907).

8. Heisenberg, W. Zur Theorie des Ferromagnetismus. Z. Physik 49, 619 (1928).

9. Weiss, P. R. The application of the Bethe-Peierls method to ferromagnetism. Phys. Rev. 74, 1493 (1948).

10. Li, Y. Y. Application of the Bethe-Weiss method to antiferromagnetism. Phys. Rev. 84, 721 (1951).

11. Anderson, P. W. Two comments on the limits of validity of the P. R. Weiss theory of ferromagnetism. Phys. Rev. 80, 922 (1950).

12. Bloch, F. Zur Theorie des Ferromagnetismus. Z. Physik 61, 206 (1930).

13. Marshall, W. The spin wave theory of antiferromagnetism. Proc. Roy. Soc. (London) A232, 69 (1955).

14. _____. Antiferromagnetism. Proc. Roy. Soc. (London) A232, 48 (1955).

15. Nagamiya, T., Yosida, K., and Kubo, R. Antiferromagnetism. Advances in Phys. 4, 1 (1955).

16. Néel, L. Propriétés magnétique de l'état métallique et énergie d'interaction entre atomes magnétiques. Ann. phys. 5, 233 (1936).

17. Van Vleck, J. H. On the theory of antiferromagnetism. J. Chem. Phys. 9, 85 (1941).

18. Anderson, P. W. Generalization of the Weiss molecular field theory of antiferromagnetism. Phys. Rev. 79, 705 (1950).

19. Smart, J. S. Molecular field treatment of ferromagnetism and antiferromagnetism. Phys. Rev. 86, 968 (1952).

20. Nagamiya, T. Theory of antiferromagnetism and antiferromagnetic resonance absorption. Progr. Theoret. Phys. 6, 342 (1951).

21. Van Vleck, J. H. Recent developments in the theory of antiferromagnetism. J. phys. et radium 12, 262 (1951).

22. Lidiard, A. B. Antiferromagnetism. Repts. Progr. in Phys. 17, 201 (1954).

23. Fowler, R. H. Statistical Mechanics (The Macmillan Company, New York, 1936), second edition.

24. Van Vleck, J. H. Electric and Magnetic Susceptibilities (Oxford University Press, London, 1932).

25. Elcock, E. W. Molecular field treatment of magnetic ordering transitions. Phys. Rev. 94, 1070 (1954).

26. Yaffet, Y. and Kittel, C. Antiferromagnetic arrangements in ferrites. Phys. Rev. 87, 290 (1952).

27. Gorter, C. J. and Haantjes, J. Antiferromagnetism at the absolute zero of temperature in the case of rhombic symmetry. Physica 18, 285 (1952).

28. Yosida, K. On the antiferromagnetism of single crystals. Progr. Theoret. Phys. 6, 691 (1951).

29. Poulis, N. J. and Hardemann, G. E. G. The threshold field phenomenon in an antiferromagnetic single crystal. Physica 20, 7 (1954).

30. _____ and Gorter, C. J. Antiferromagnetic crystals. Progr. Low Temp. Phys. 1, 245 (1955).

31. Smart, J. S. Molecular field treatment of antiferromagnetism. Revs. Modern Phys. 25, 327 (1953).

32. Greenwald, S. and Smart, J. S. Crystal structure transitions in antiferromagnetic compounds at the Curie temperature. Phys. Rev. 82, 113 (1951).

33. Néel, L. Études sur le moment et le champ moléculaire des ferromagnétiques. Ann. phys. 8, 237 (1937).

X APPENDICES

Appendices A, B, C and D are included in the Ph. D. thesis by Thomas James Hendrickson, which may be obtained from the Iowa State College Library, Ames, Iowa.

I-II AND

1—119

THIS PAGE

WAS INTENTIONALLY

LEFT BLANK